Al-Khwarizmi Engineering Journal, Vol. 19, No. 3, September, (2023)
P. P. 1- 22

Al-Khwarizmi Engineering Journal

Removal of Ciprofloxacin Antibiotic from Synthesized Aqueous Solution Using Three Different Metals Nanoparticles Synthesized Through the Green Method

Abdelmalik Milad Shakorfow* **Najah Al Mhanna****
Mohammed A. Atiya*** **Ahmed K. Hassan****** **Fatimah Q. Kadhim*******
Zainab A. Mahmoud****** **Azza Hashim Abbas*********

**Elmergib University / Libya*
*** German University of Technology in Oman/ Oman*
****,*****,******Department of Biochemical Engineering/ Al-khwarizmi College of Engineering/ University of Baghdad/ Baghdad/ Iraq*
*****Environment and Water Directorate/ Ministry of Science and Technology/ Baghdad/ Iraq*
********School of Mining and Geosciences/ Nazarbayev University/ Kazakhstan*
*Email: Dr_Eng.Malik@Yahoo.Co.Uk
**Email: najah.almhanna@gutech.edu.om
***Email: atiya@kecbu.uobaghdad.edu.iq
****Email: ahmedkhh71@gmail.com
*****Email: qaf2622@gmail.com
Corresponding Author: ******Email: Zainab.amahmoud@gmail.com
*******Email: azza.hashim@nu.edu.kz

(Received 30 October 2022; Accepted 6 February 2023)
https://doi.org/10.22153/kej.2023.02.002

Abstract

This study investigates the possibility of removing ciprofloxacin (CIP) using three types of adsorbent based on green-prepared iron nanoparticles (Fe.NPs), copper nanoparticles (Cu. NPS), and silver nanoparticles (Ag. NPS) from synthesized aqueous solution. They were characterized using different analysis methods. According to the characterization findings, each prepared NPs has the shape of a sphere and with ranges in sizes from of 85, 47, and 32 nanometers and a surface area of 2.1913, 1.6562, and 1.2387 m^2/g for Fe.NPs, Cu.NPs and Ag.NPs, respectively. The effects of various parameters such as pH, initial CIP concentration, temperature, NPs dosage, and time on CIP removal were investigated through batch experiments. The results showed that 10 mg/L CIP was removed by 100%, 92% and 79% within 180 min using Fe.NPs, Cu.NPs, and Ag.NPs respectively. In addition to this, kinetic models of the adsorption and mechanism of CIP removal were studied. The cinematic analysis demonstrated that adsorption is a physics adsorption mechanism with an energy of 0.846 $kJ.mol^{-1}$, 1.720 $kJ.mol^{-1}$, and 3.872 $kJ.mol^{-1}$, while the low activation energies of 17.660 $kJ.mol^{-1}$, 13.221 $kJ.mol^{-1}$, and 14.060 $kJ.mol^{-1}$ for Fe.NPs, Cu.NPs, and Ag.NPs respectively. The kinetic removal process follows a pseudo-first-order model following a physical diffusion-controlled reaction. The data on adsorption was analyzed using the Langmuir, Freundlich, Temkin, and Dubinin models, as well as thermodynamic factors, indicating that the process is appropriate and endothermic sorption. The most practical adsorbent was Fe.NPs

Keywords: *Removal Ciprofloxacin, Green synthesis, Iron, Copper, Silver, Nanoparticles, Adsorption, Thermodynamics, and Kinetics.*

1. Introduction

Antibiotic waste in water supplies is one of the most significant challenges facing communities today, especially when it is discovered in drinking water sources [1][2]. The presence of these medicines in large quantities has a negative impact on the ecology [3][4]. In the present time, the world emits harmful substances into the environment either directly or after chemical changes [5]. Antibiotics are widely used because they treat a wide range of bacterial infections in humans, animals, birds, and fish [6].

Ciprofloxacin is a type of antibiotic that is commonly used as a treatment for a variety of bacterial infections around the world [7]. Fluoroquinolones have been found in aquatic environments in concentrations ranging from "1-100 mg/L" [8]. The broad-spectrum fluoroquinolone pharmaceutical medication that is frequently utilized is "Ciprofloxacin ((1-Cyclopropyl-6-fluoro-4-oxo-7-(piperazine-1-yl)-1,4-dihydroquinoline-3-carboxylic acid hydrochloride hydrate)" [8]. Drug contamination is also caused by trash from hospitals, housekeepers, and human excretion [9]. Non-target persons and biota are at risk from improper disposal of antibiotic-loaded pharmaceutical wastewater [10][11].

Many approaches, such as advanced oxidation processes (AOPs) bioremediation, ozonation, chlorination, and others, have been proposed to treat CIP-contaminated wastewater. However, these methods have a number of drawbacks, including poor removal, difficult procedures, and significant energy needs [1]. Furthermore, multiple studies have suggested that chlorinating antibiotic-contaminated wastewater could form a carcinogenic byproduct. As a result, it is crucial to convert antibiotic compounds to safe compounds before discharging them into water systems [12]. Traditional treatment approaches do not completely eradicate antibiotics because of their environmental stability and extended breakdown durations [13] [14]. Antibiotic wastewater treatment necessitates substantial technological resources, with the adsorption process being seen as the most promising method because it is effective, simple to implement, and technically advanced.

To remove pollutant molecules (adsorbates) from contaminated solutions, the procedure employs natural and synthetic materials (sorbents, adsorbents, and biosorbents) [15]. In the adsorption process, the adsorbent material chosen is a critical aspect in obtaining the required efficiency in terms of pollutant removal and cost [16][17]. Before being used, the sorbents must have been tested in this environment to ensure that they can perform adsorption for a variety of pollutants. These tests must also consider the accessibility and cost-effectiveness of the tested adsorbents [18][10].

Several materials are available to use as adsorbents, like activated carbon, natural clay (modified bentonite), and polymer-based materials [2]. Researchers have recently proposed using generated trash as an adsorbent in a creative or improved form [20][21]. Metal nanoparticles (NPs) prepared by the green synthesis method using plant extracts have become widely used as adsorbents in the removal of medicine from wastewater [22]. In addition. The green synthesis method is eco-friendly, cost-effective, and easy to develop on a large scale. Green synthesis usually consists of three steps: (1) solvent media selection; (2) environmentally friendly reduction agents' selection; and (3) stable, non-toxic compound nanoparticle selection [19]

Moreover, iron (Fe.NPs) and copper (Cu.NPs) nanoparticles are lower cost, have wide viability [25], simple to produce [26], are environmentally friendly, and have extensive dispersion of reactive surface sites [27] [28], while silver nanoparticles (Ag.NPs) are widely used as antibacterials, sensors, catalysts, and adsorbents [29] [30]. In this study, the adsorption of ciprofloxacin from synthesis wastewater has been successfully employed using Iron nanoparticles (Fe.NPs), Copper nanoparticles (Cu.NPs), and silver nanoparticles (Ag.NPs) nanoparticles have been successfully studied. In addition, "Pseudo-first order, Pseudo-second order, Elovichs, and Behnajady- Modirshahla- Ghanbary (BMG)" models were used to evaluate the adsorption kinetics. The ciprofloxacin analysis was investigated using the Langmuir, Freundlich, Temkin, and Dubinin- models as well as the thermodynamic parameters [31].

2. Materials and Methods

2.1 Reagents and chemicals

The Ministry of Industry (Ibn Sina Centre) provided the ciprofloxacin used in this study with the characteristics of the drug as (molecular wight = 385.8 g/gmol, color: whit, purity: 99.9% and λmax = 276 nm), while green tea leaves purchased from the local market in Iraq. A spectrophotometer (UV/VIS 1800 SHIMADZU, Japan) was used to

measure the maximum wavelength α (nm). Figure 1 illustrates the chemical structure of the drug.

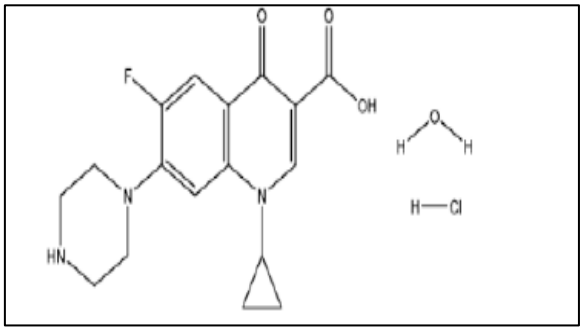

Fig. 1. The CIP structure.

2.2 Preparation of the Adsorbent

The " Fe.NPs, Cu.NPs, and Ag.NPs" nanoparticles were made using the same processes as those used in earlier investigations [34][35], with the following modifications:
"Green tea" leaf extract was made with "20.0 g of green tea and 300 mL of distilled water (DW). The mixture was preheated on a magnetic stove at 85°C for half an hour. After that the suspended green tea impurities were filtered with" 0.45 µm filter paper and stored at 4°C for further use. By adding 3.25 g of FeCl3, 4.996g of CuSO4.5H2O, and 3.4g of AgNO3 salt to 200 mL of DW, a solution of 0.10 M FeCl3, 0.1 M CuSO4.5H2O, and 0.1 M AgNO3 was prepared. After slowly adding the prepared tea extract to each salt solution, the color of each solution changed from light yellow to black for iron, from white to green light for silver, and finally to a dark brown, and from colorless to brownish yellow, and finally to black for copper, the reduction of metal ions to zero valent for example Fe (+3) to Fe (0) when we added the plant extract {this extract is very rich in polyphenols compounds which are played as reducing agents for metal ions}, and from colorless to brownish yellow after that the pH was adjusted to 6 iron [36], 9 for copper and silver [37] [38], and the mixture was continually stirred for 15 minute. The NPs precipitate was collected using vacuum filtration and immediately washed with water and ethanol. Green Fe.NPs, Cu.NPs, and Ag.NPs were dried at room temperature overnight before being ground into fine powders.

2.2 Characterization of NPs

The prepared NPs were characterized using SEM images were taken with a" TESCAN-Vega3 model" to detect morphology and particles size of prepared NPs. The functional groups of Cu, Ag and Fe.NPs were identified by FTIR (IRAffinity, Shimadzu, Japan). A" Brunauer–Emmett–Teller (BET)" application was used to compute the specific surface area, pore size, and pore volume of NPs. Nanoparticle stability was determined using a "zeta potential analysis", and the size and "surface morphology" of the NPs determined by atomic force microscopy (AFM).

2.3 Experiments of Adsorption

Before adding nanoparticles, a stock solution of 10 mg/L of ciprofloxacin solution was prepared, and the pH. A batch of experiments was carried out to examine the adsorption process of ciprofloxacin on prepared NPs. Several operating parameters were met in the studies, including a pH (2–10), a dosage range of 0.1–1 g/L for Fe.NPs, Cu.NPs, and Ag.NPs, a contact time range of up to 180 minutes, contaminant concentrations of (2–15 mg/L), and temperatures of (20–50 °C). The ciprofloxacin solution was supplemented with a particular amount of targeted NPs, and then agitated at 300 rpm in a closed system. 0.1 M H2SO4 and 0.1 M NaOH were used to bring the pH of the CIP solution up to the desired level. The temperature was kept constant, and each parameter's optimal value was recorded. Samples)10 ml(were obtained at various times throughout the experiments, and the change in CIP concentration was determined through a UV/VIS spectrophotometer. The ability of Fe.NPs, Cu.NPs, and Ag.NPs to extract antibiotic pollutants from aqueous solutions was assessed using R% removal efficiency and Qe mg/g adsorbent capacity values using the following two formulas [34] [33].

$$\%\, Removal = \frac{C_o - C_t}{C_o} \times 100 \quad \ldots(1)$$

$$Q_e = (C_o - C_e) \times \left(\frac{V}{W}\right) \quad \ldots(2)$$

Where C_o is initial CIP concentration (mg/L), C_t is the concentration after adsorption being start (mg/L) and C_e is equilibrium concentration (mg/L). V is the volume of CIP solution (L) and W is the Wight of CIP (g).

3. Results and Discussions

3.1 Characterization of NPs

A scanning electron microscope (SEM) was used to illustrate the shape and distribution of the

nanoparticles. According to the SEM of Fe.NPs that is presented in Figure (2a), the adsorbent surface is rough and contains many different disorganized aggregates. On the surface of the Fe.NPs wall, there were a number of grooves and deep ravines. The morphologic characteristics of the surface of the Fe.NPs are generally favorable because they offer active sites and a large surface area for the molecules that are adsorbed. Figures (2b-c) show SEM images of the generated Cu.NP and silver nanoparticles (Ag-NP). SEM pictures revealed the shape and distribution of these components. Because polyphenols are present on the surface of nanoparticles, irrelevant spherical nanoparticles were discovered that were compatible with copper- and silver-based preparations employing extracts of green tea leaves

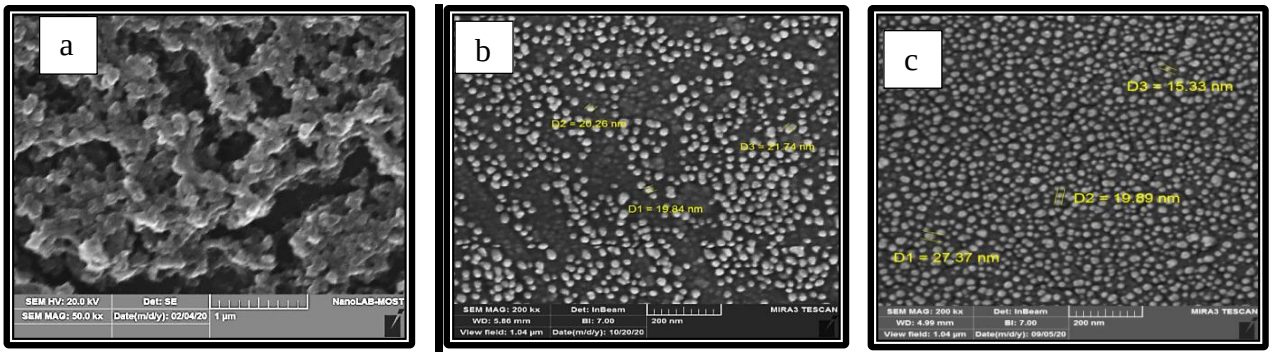

Fig. 2. Scanning electron microscope (SEM) micrograph of (a) Fe.NPs, (b) Cu.NPs, and (c) Ag.NPs

The Fe.NPs FTIR spectrum is shown in Figure 3a. The " FTIR analysis of Fe.NPs reveals a functional group of O – H at 3364 cm-1, indicating the existence of polyphenols [25] and the C=O appeared at 1635 cm-1 also referring to the presence of polyphenols. The functional groups of C-H, C-O-C and C=C appeared at 2924 cm-1, 1035 cm-1, and 1367 cm-1 belong to the oxidized polyphenols on the produced Fe.NPs. Polyphenols are thought to behave as antioxidants in Green Tea Extract as well. In the FTIR analysis of Cu.NPs Figure (3b), the presence of polyphenols is indicated by this the peak at 3411 cm-1 that belong to O-H stretching, along with the association between C-H asymmetrical stretching and certain signals in 2948, 1782, 1615, and 1029 cm-1, C=O of aromatic rings, C=C stretch, and C-OH bending respectively. Based on FTIR measurements, Ag.NPs with a wave range of 3371cm-1 to 1021cm-1 show characteristic peaks. Wide and strong absorption peaks were identified between 3371 and 3259 cm-1, indicating the presence of polyphenols and extended hydroxyl vibrations (O-H). Carbonyl C=O was detected by a significant absorption, with C=C stretching frequencies peaking between 1639 and 1634 cm-1. Figure 3c shows the vibration of the O-H delay, which could be caused by the other pits between 1160cm-1.

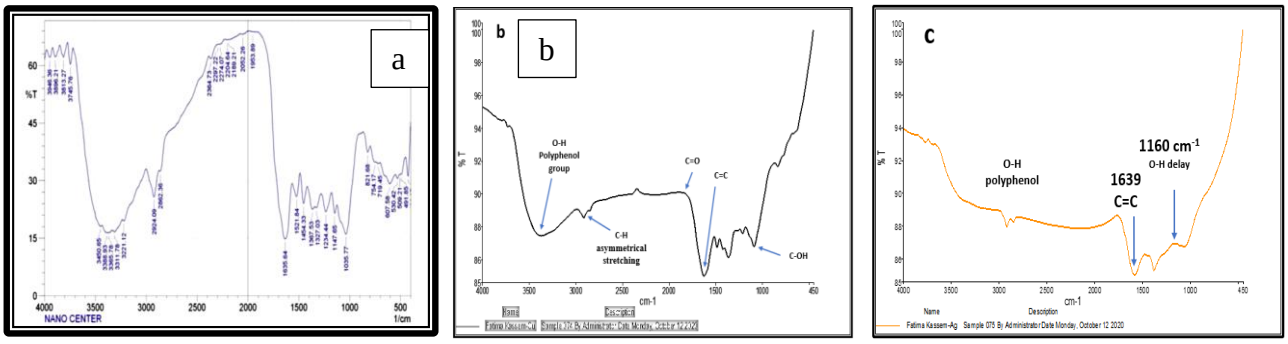

Fig. 3. FTIR spectrum of (a) Fe.NPs, (b) Cu.NPs, and (c) Ag.NPs nanoparticles.

The size and surface morphology of Fe.NPs, Cu.NPs, and Ag.NPs nanoparticles were investigated with the help of a atomic force microscopy (AFM). The average nanoparticle size

for according to the AFM for iron, copper, and silver nanoparticles were (85, 47, and 32 nm), respectively, as shown in Figures (4a-c). Figures (5a-c) illustrates the AFM results of Fe.NPs, Cu.NPs, and Ag.NPs nanoparticles.

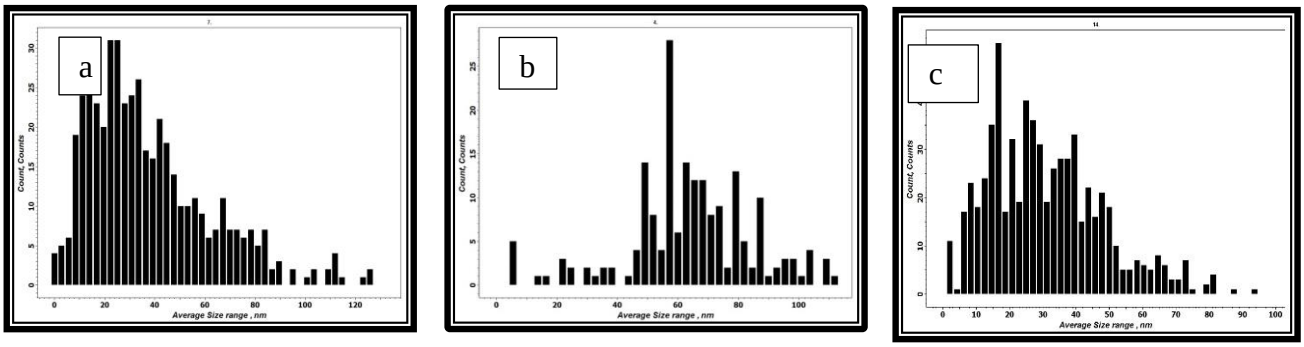

Fig. 4. AFM images of nanoparticles composed of (a) Fe.NPs, (b) Cu.NPs, and (c) Ag.NPs.

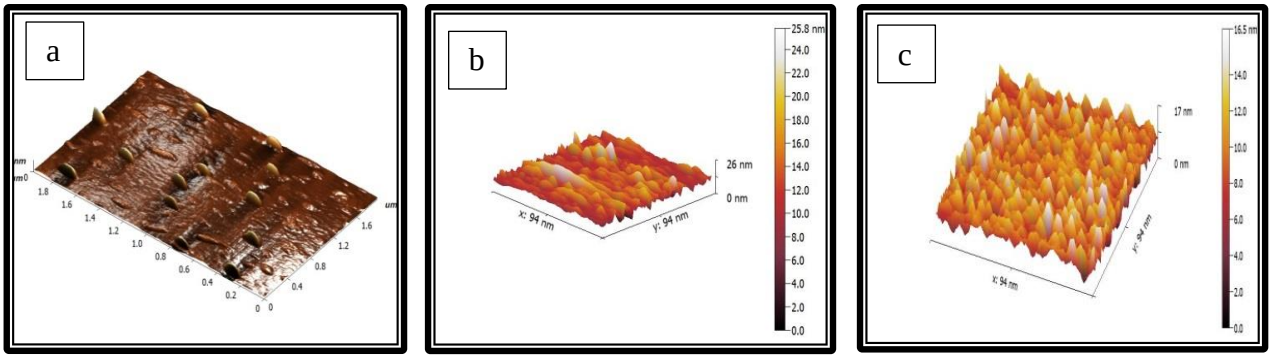

Fig. 5. Nanoparticles of (a) Fe.NPs, (b) Cu.NPs, and (c) Ag.NPs examined by atomic force microscopy.

Nanofluid stability was determined using a zeta potential analysis technique, as shown in Figure 6a-c, the zeta potential values were -19.34 mV for Fe.NPs, -17.5 mV for Cu.NPs, and -29.1 mV for Ag.NPs, it was proven that the nanoparticles were more agglomerative.

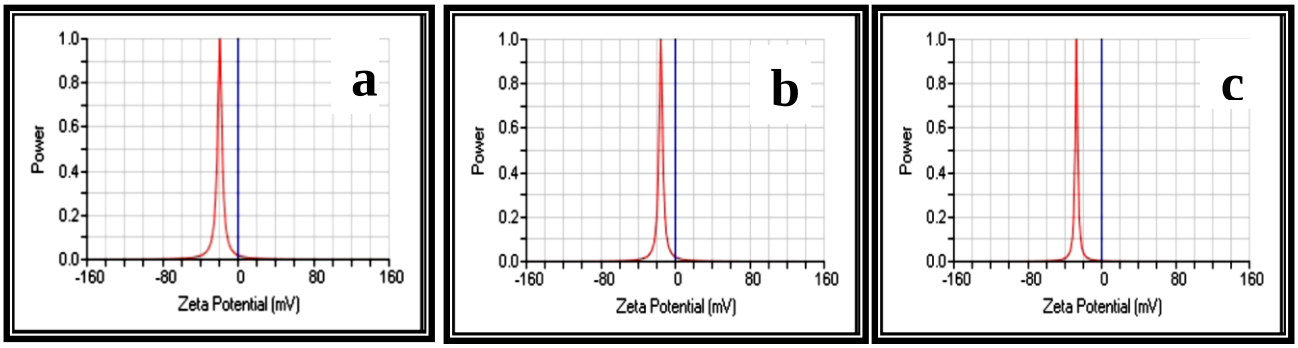

Fig. 6. Zeta potential of (a) Fe.NPs, (b) Cu.NPs, and (c) Ag.NPs nanoparticles.

Blumenauer-Emmer-Teller (BET) data are shown in Table 1, which explain and clarify the surface area. Pore sizes for iron, copper, and silver nanoparticles were 34.8651 nm, 8.2568 nm, and 5.1843 nm, respectively. According to the IUPAC, pore sizes between 20 and 50 nm are considered mesoporous.

Table 1,
The BET parameters for Fe.NPs, Cu.NPs, and Ag.NPs nanoparticles.

Nanoparticle	BET parameters BET(m^2/gm)	Volume of pores(cm^3/gm)	Size of pores (nm)
Fe.NPs	2.1913	0.0191	34.8651
Cu.NPs	1.6562	0.00839	8.2568
Ag.NPs	1.2387	0.000618	5.1843

3.2 CIP removal under various conditions

In a closed system, the removal of ciprofloxacin by Fe.NPs, Cu.NPs, and Ag.NPs" was studied, and the removal percentage was determined under various experimental conditions. UV-Vis at a wavelength of 276 nm was used to take samples and analyze them at various time intervals. "Initial pH was set to 2.5, 3, 4, 5, 7, 8, 9, and 10, initial ciprofloxacin concentrations were set to 2, 5, 10, and 15 mg/L, Fe.NPs, Cu.NPs, and Ag.NPs doses were set to 0.1, 0.25, 0.5, 0.75, and 1 g/L, and the solution temperatures were set to 20, 30, 40, and 50 °C. Eq. 1 was used to determine the ciprofloxacin removal performance.

3.2.1 Effect of adsorbent

The adsorbent dosage is an important factor to consider due to its role in demonstrating the catalyst's capacity to deal with a particular initial contaminant concentration. The effect of Fe.NPs, Cu.NPs, and Ag.NPs dosages on ciprofloxacin elimination is shown in Figures 7a-c, respectively. The ciprofloxacin removal was raised from 18% to 70% when Fe.NPs were used, and the adsorption dosage was increased from 0.1 to 1.0 g/L, while it improved from 20% to 54% when Cu.NPs were used, and from 18% to 45% when Ag.NPs were used. Higher Fe.NPs, Cu.NPs, and Ag.NPs for ciprofloxacin adsorption improved the removal rate and effectiveness while maintaining the other parameters (drug concentration, pH, temperature, and contact time). This is because the total area and active site have both increased. [41]. For iron, copper, and silver nanoparticles, doses of 0.5g/L, 0.75g/L, and 1 g/L were chosen as the optimal values. A similar result was indicated by [3], [4].

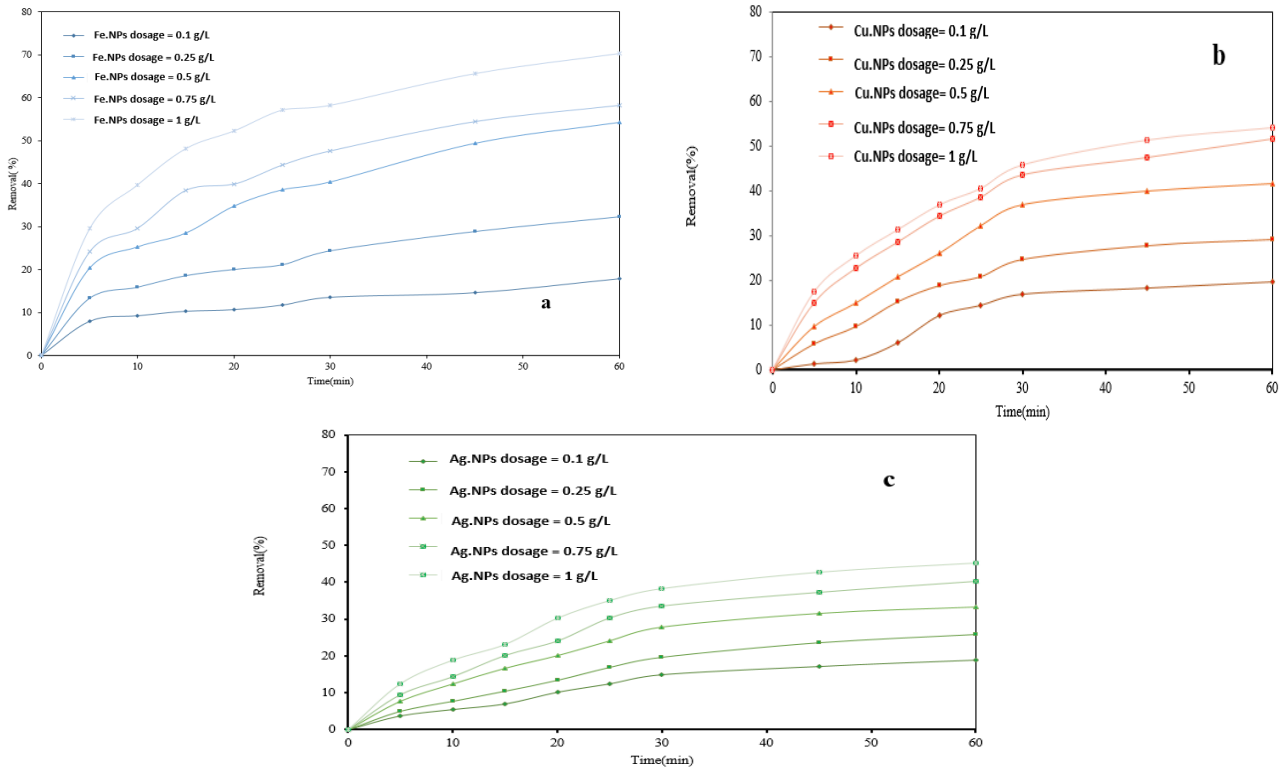

Fig. 7. Effect of "(a) Fe.NPs , (b) Cu -NPs, and (c) Ag.NPs doses at pH =3, 10 mg / L ciprofloxacin, 40°C, 300 rpm and contact time of 60 min".

3.2.2 Effect of temperature

At temperatures ranging from 20 to 50 °C, the influences on ciprofloxacin removal efficiency were investigated. The efficiency of ciprofloxacin at various temperatures is shown in Figures 8 a-c. Since Fe.NPs removed 36 percent, 40 percent, 54 percent, and 53 percent of ciprofloxacin at 20, 30, 40, and 50°C, respectively, 43 percent, 44 percent, 78 percent, and 49 percent with Cu.NPs, and Ag.NPs removed 31 percent, 40 percent, 52 percent, and 45 percent with Ag.NPs, it is possible to conclude that the removal rate of ciprofloxacin is influenced by temperature and increased with increase in temperature. This could be due to an increase in the number of sorption sites generated because of the breaking of some internal bonds near the active surface sites of the adsorbent. Furthermore, the increasing temperature may increase the mobility of the CIP, enabling it to penetrate further. As a result, there are more medicines interacting with adsorbent active surfaces." For Fe.NPs, Cu.NPs, and Ag.NPs", the optimal temperature was 40°C. Similar observations were noted by [5].

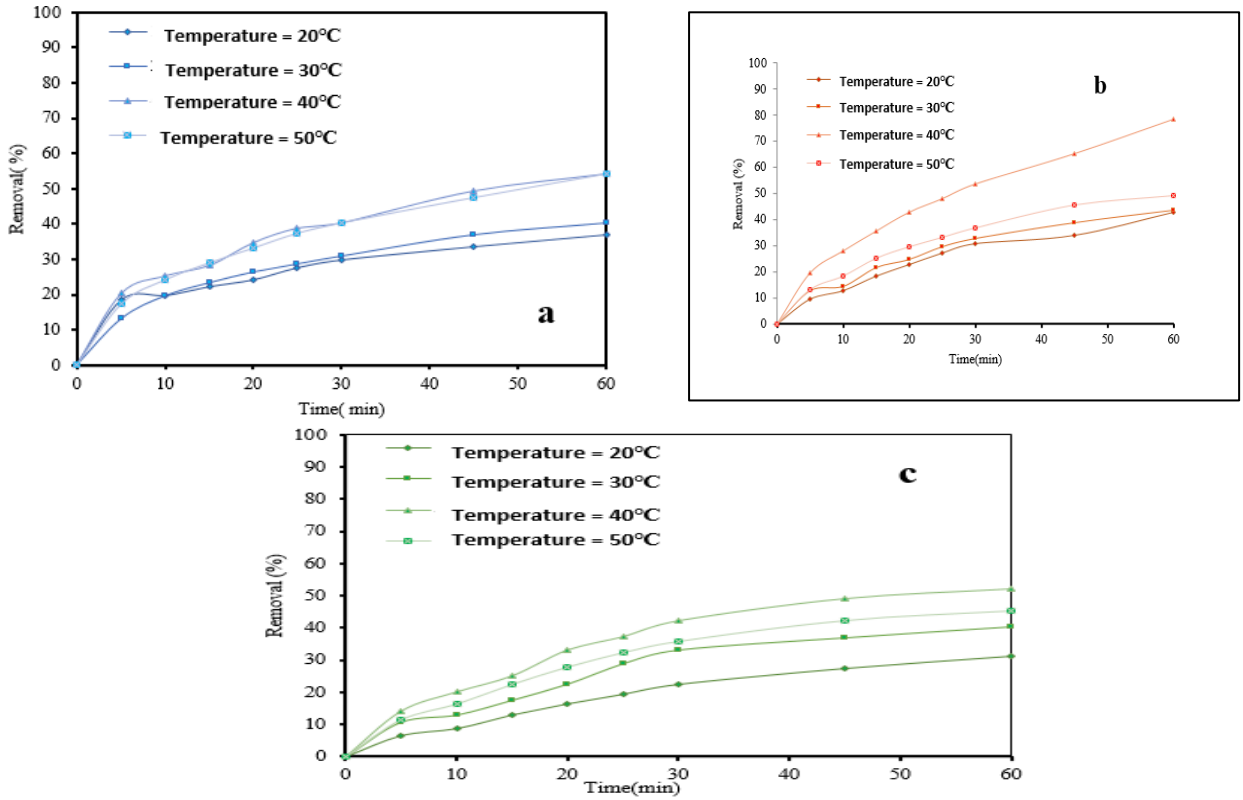

Fig. 8. The temperature effect on ciprofloxacin removal onto various adsorbents at (10 mg/L of CIP), 300 rpm, one hours (a) 0.5 g/L and pH=10 of Fe.NPs, (b) 0.75 g/L and pH=4 of Cu.NPs, and (c) 1 g/L, and pH=4 of Ag.NPs.

3.2.3 Effect of pH

As shown in Figures (9 a-c) , the influence of pH is compared to ciprofloxacin adsorption by NPs. Two reasons were identified in the studies as possibly accounting for the increased ciprofloxacin adsorption: (1) At low pH, the concentrations of H+ in the solution were very high, enhancing the electrostatic pull between H+ in the solution and the adsorbent surface, resulting in competition for adsorption sites between H+ and CIP+; (2) at higher (pH10), H+ of active groups can be easily dissociated and provide more adsorption sites [44]. In acidic environments, antibiotic molecules are positive, with 99% of ciprofloxacin molecules being (cationic), 10% being ciprofloxacin +, and 95% being anionic. When the pH is 7, ciprofloxacin 0" predominates (zwitterion). A physi-sorption reaction between ciprofloxacin molecules and the active sites of" Fe.NPs, Cu.NPs, and Ag.NPs "may occur at pH = 10, 4, and 4, respectively. Figure (9 a) demonstrates that Fe.NPs improved the efficacy of removal at a range of pH values (2.5, 3, 4, 5, 7, 8, 9, and 10) for 60 min, with increases of 21%, 54%, 69%, 72%, 70%, 68%, 81%, and 92%, respectively. While Figure (9 b)

showed that the percentage removal of ciprofloxacin by Cu.NPs increased at acidic pH and then decreased at basic pH as 36 percent, 51 percent, 78 percent, 50 percent, 43 percent, and 32 percent, a similar result was indicated by [6], [7], [8]. Figure (9 c) explains the removal of ciprofloxacin by Ag.NPs and the same observation was made at 37%, 45%, 52%, 48%, 43%, 30%, 23%, and 21%. The optimum values of pH for the removal" ciprofloxacin by Fe.NPs, Cu.NPs, and Ag.NPs are 10, 4, and 4" respectively.

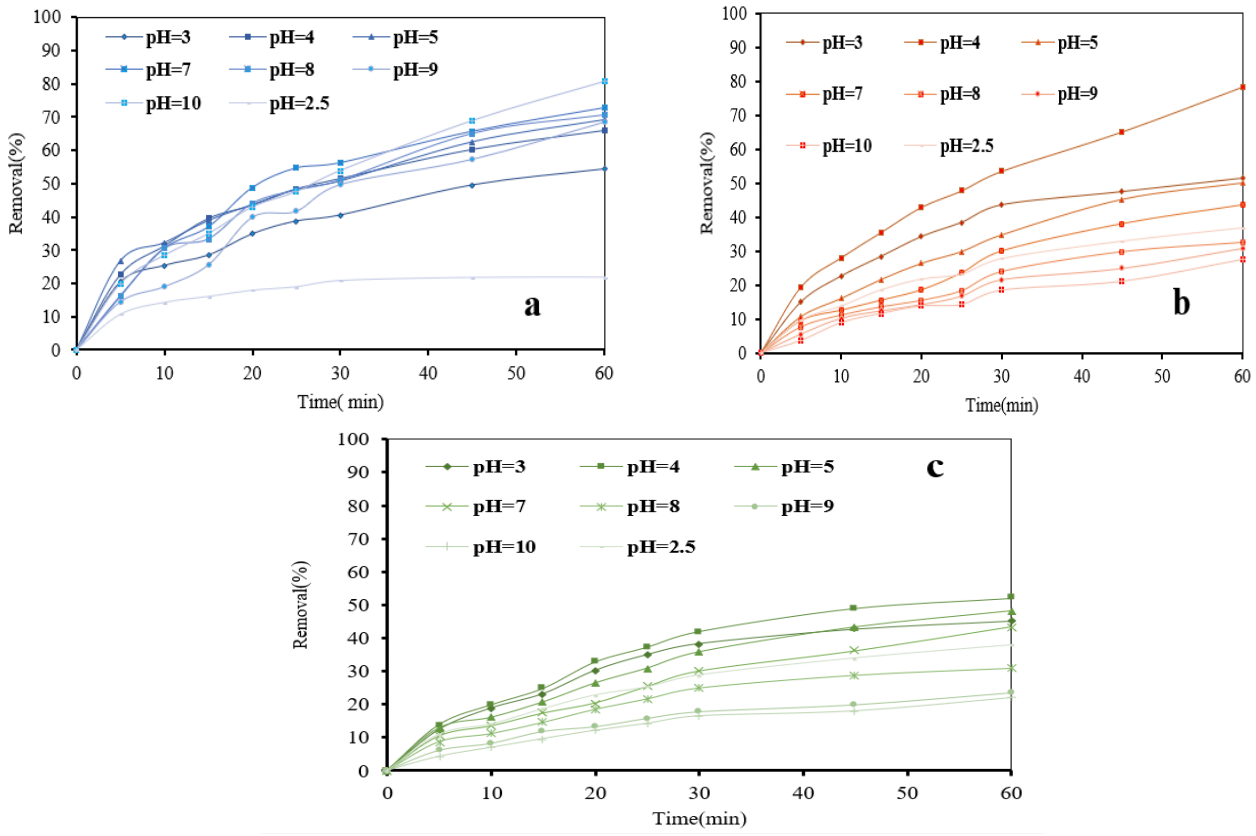

Fig. 9. The effect of pH on the removal of " ciprofloxacin at 10 mg/L of concentration", one hours, and 300 RPM onto (a) 0.5 g/L, pH10 and 40℃ of Fe.NPs, (b) 0.75 g/L, pH 4, and 40℃ of Cu.NPs, (c) 1 g/L, pH4, and 40℃.

3.2.4 Effect of initial concentration

Figures (10 a-c) represent the effect of drug concentration on removal efficiency for ciprofloxacin adsorption in the range of 2, 5, 10, and 15 mg/L. By employing "Fe.NPs, Cu.NPs, and Ag.NPs", the removal percentage decreased from 100% to 81% ,81% to 39 % for Fe.NPs, while Cu.NPs showed 99 % to 83 %, 78 % to 42 %, and Ag.NPs removal efficiency decreased from 57 % to 54 %, 52 %, to 48 % as the concentration of ciprofloxacin increased. Other researchers' observations [34] have similar results to this study. The initial ciprofloxacin concentration for more active sites of Fe.NPs, Cu.NPs, and Ag.NPs because they are likely to rise, resulting in ciprofloxacin molecule adsorption competition [42]. The driving force is accelerated, and the resistance to mass transfer is reduced, when the first concentration is high. Within one hour of the process, the optimal value for the initial CIP concentration with all adsorbents was "10mg/L", and the removal of ciprofloxacin was 81 %, 78 %, and 54 %.

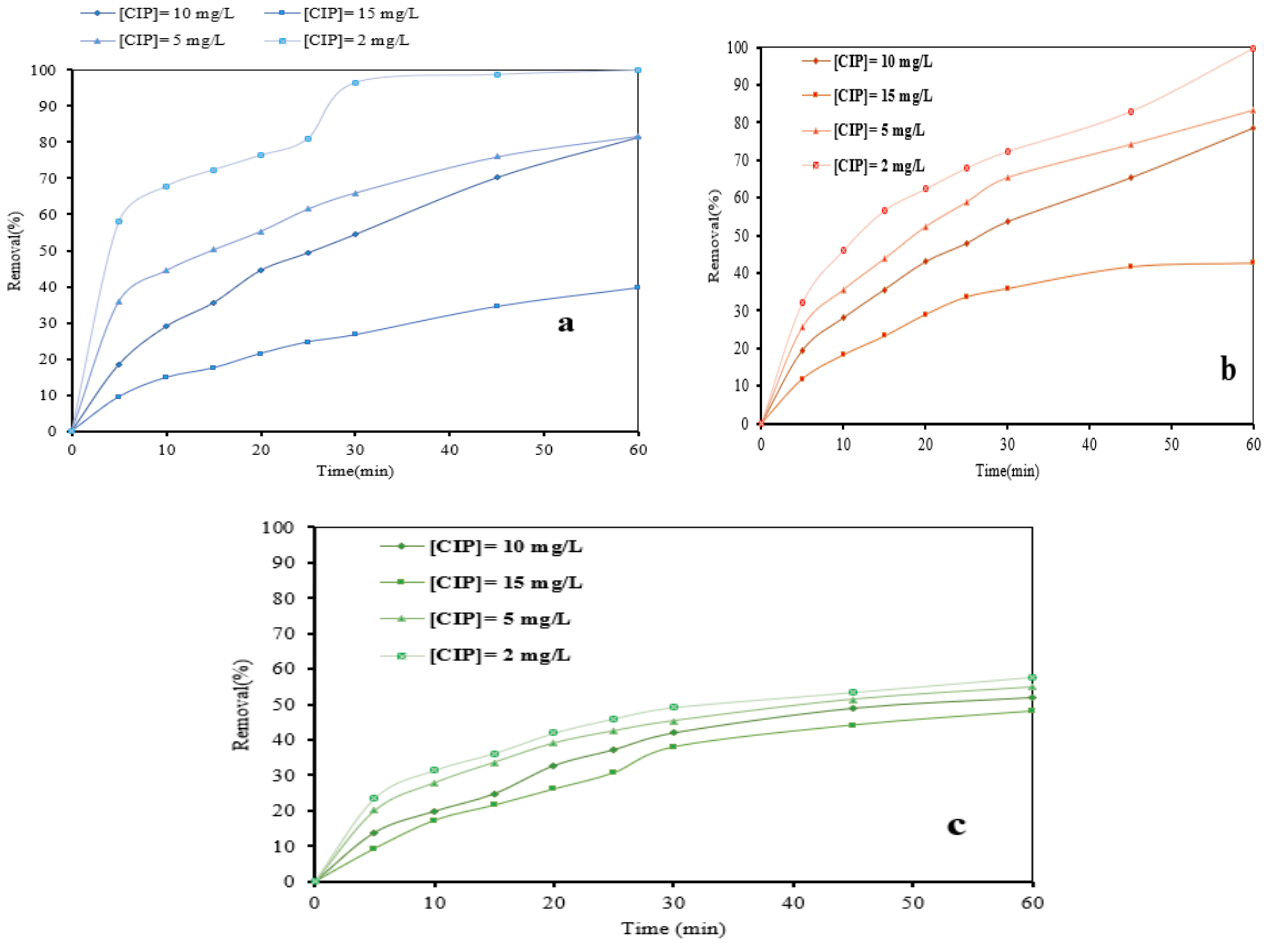

Fig. 10. The effect of the ciprofloxacin concentration at 300 rpm, one hour, and T = 40°C (a) Fe- NPs of 0.5g/L, pH10, (b) Cu.NPs of 0.75g/L, pH4, and (c) Ag.NPs of 1g/L, pH4.

3.2.5 Effect of contact time

To indicate the equilibrium point, a time effect is an important parameter of the sorption process. At pH 4, 7, and 10, the effect of increased contact time is seen in Figure 11. With more time, the batch system's ciprofloxacin removal efficiency improves. The process was initially fast because of the high driving force at high ciprofloxacin level, but when the amount of non-adsorbed " ciprofloxacin "molecules in the adsorbent active site decreased, the removal rate declined for all pH levels [49]. The " ciprofloxacin removal" at pH 4, 7, and 10 for one hour was "59%, 72%, and 81% by using Fe.NPs, and 80%, 43%, and 27% for Cu.NPs", while the removal of ciprofloxacin was 53%, 43%, and 22% for Ag.NPs. The " ciprofloxacin removal after 180 min. at 4, 7, and 10" were 92%, 93%, and 100% with Fe.NPs, and 92%, 70%, and 50% with Cu.NPs, while the removal efficiency was 79%, 67%, and 42% by using Ag.NPs.

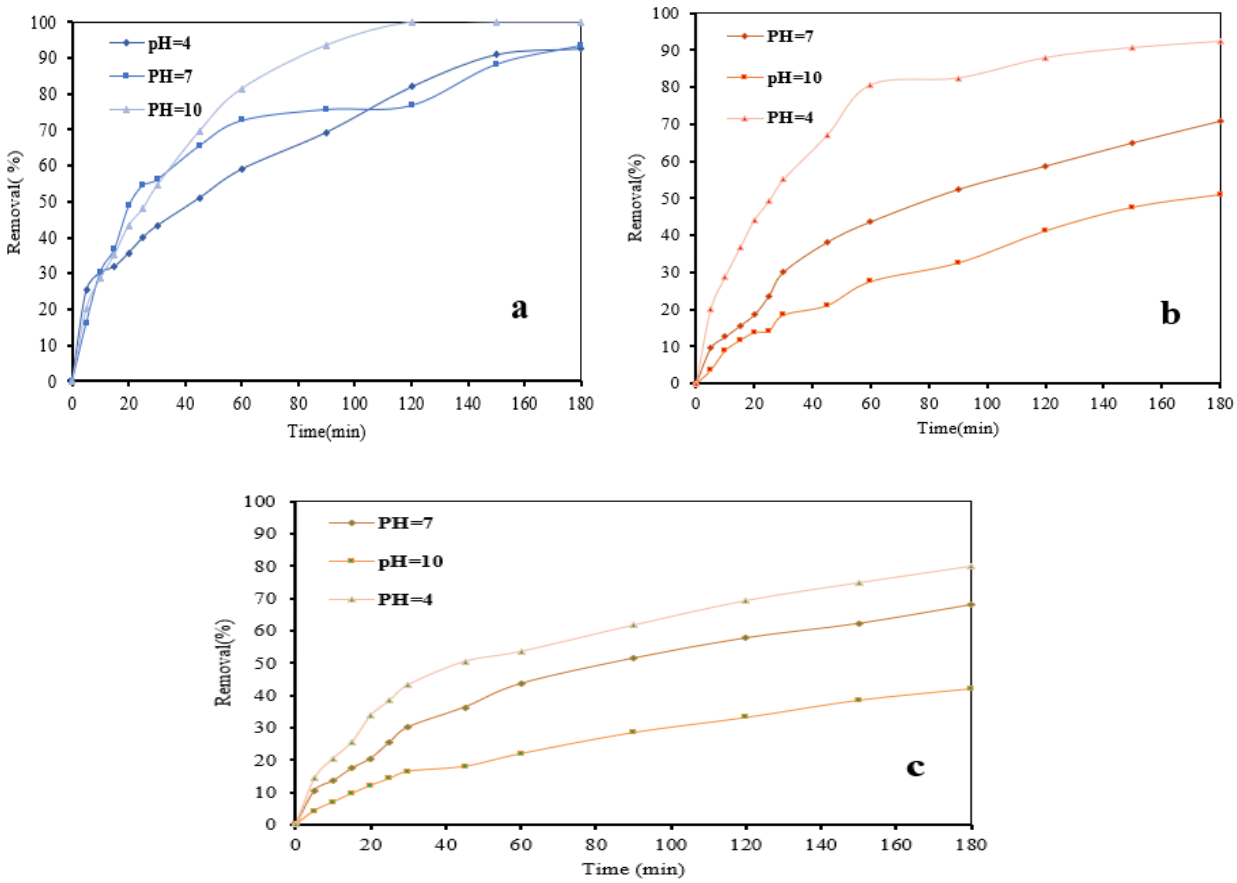

Fig. 11. Time effect at different pH (CIP conc.10 mg/L, 0.5 g/L Fe.NPs, 0.75 g/L Cu.NPs, and1 g/L Ag.NPs, with constant temperature of 40 °C.

4. Adsorption Mechanism

Equations (3) and (4) were used to determine the mechanism of the sorption process. (3) and (4) [9][5] [10].

Kinetics of intraparticle diffusion:

$$q_{t} = K_{id}\, t^{0.5} + C \qquad \ldots(3)$$

Kinetic model of liquid film diffusion:

$$Ln\,\frac{1-q_t}{q_e} = -K_{fd} \times t \qquad \ldots(4)$$

The intraparticle diffusion constants are Kid (mg/g min0.5) and C (mg/g). The thickness of the boundary layer is indicated by the C parameter, while the liquid film diffusion constant is shown by K_{fd} (m^{-1}). When the linear trend fit from the qt vs $t^{0.5}$ as presented in Figures (12a-c) passes the point of origin of the parameter C = 0, that mean the intraparticle diffusion is the limiting rate. In Figure (12a-c), the slop and intercept of the plot of ln (1-qt/qe) versus t correspond to K_{fd} and C. Tables (2), (3), and (4) demonstrate the results of "intra-particle and film diffusion" experiments at different ciprofloxacin initial concentrations (4). The linear model in Figures (12a-c) and (13a-c) did not pass through the origin, implying that the thickness of the boundary layer controls the adsorption process. The high values of the regression coefficients suggest that liquid film diffusion plays a more crucial role, and that a greater concentration gradient causes ciprofloxacin molecules to diffuse more quickly across the boundary layer surrounding the adsorbent. The C values strongly suggest that intr-aparticle diffusion was also utilized in the sorption process. In addition to diffusion, several adsorption mechanisms control the rate of intra-particle diffusion. Such aberrations have been described in a number of scientific studies [51], [10].

Table 2,
Model and liquid film diffusion on Fe.NPs at different CIP conc. for the intra-particle adsorption mechanism.

CIP (mg/L)	Intra-particle Diffusion			Liquid Film Diffusion		
	K_{id} (mg/g.min$^{0.5}$)	C(mg/g)	R^2	K_{fd} (min^{-1})	C(mg/g)	R^2
15	1.2389	-0.3418	0.995	0.0074	-0.0581	0.9644
10	1.7863	-0.6041	0.9937	0.0186	-0.066	0.9933
5	0.9729	0.7791	0.9675	0.022	-0.2507	0.9414
2	0.4327	0.6789	0.8761	0.0467	-0.4272	0.8984
Average R^2			0.9580			0.9503

Table 3,
Model and liquid film diffusion on Cu.NPs at different CIP concentrations for the intra-particle adsorption mechanism.

CIP (mg L^{-1})	Intra-particle Diffusion			Liquid Film Diffusion		
	K_{id} (mg g^{-1}.min$^{-0.5}$)	C(mg/g)	R^2	K_{fd} (min^{-1})	C(mg. g^{-1})	R^2
15	0.7982	0.0498	0.9727	0.0318	-0.1481	0.9584
10	1.349	0.3249	0.9963	0.0308	-0.0212	0.9834
5	1.4592	0.1978	0.9931	0.0341	-0.1047	0.9926
2	1.6584	0.559	0.9895	0.0398	-0.0662	0.9475
Average R^2			0.9879			0.9704

Table 4,
Model and liquid film diffusion on Ag.NPs at different CIP conc. for the intra-particle adsorption mechanism.

CIP (mg/L)	Intra-particle Diffusion			Liquid Film Diffusion		
	K_{id} (mg / g.min$^{0.5}$)	C(mg /g)	R^2	K_{fd} (min^{-1})	C(mg /g)	R^2
15	0.8465	-0.358	0.979	0.0257	-0.0521	0.9848
10	0.7216	-0.0958	0.9826	0.0298	-0.0952	0.9813
5	0.719	0.3928	0.9731	0.0681	-0.1973	0.9852
2	0.6123	0.4693	0.9594	0.0405	-0.2339	0.9801
Average R^2			0.9735			0.9828

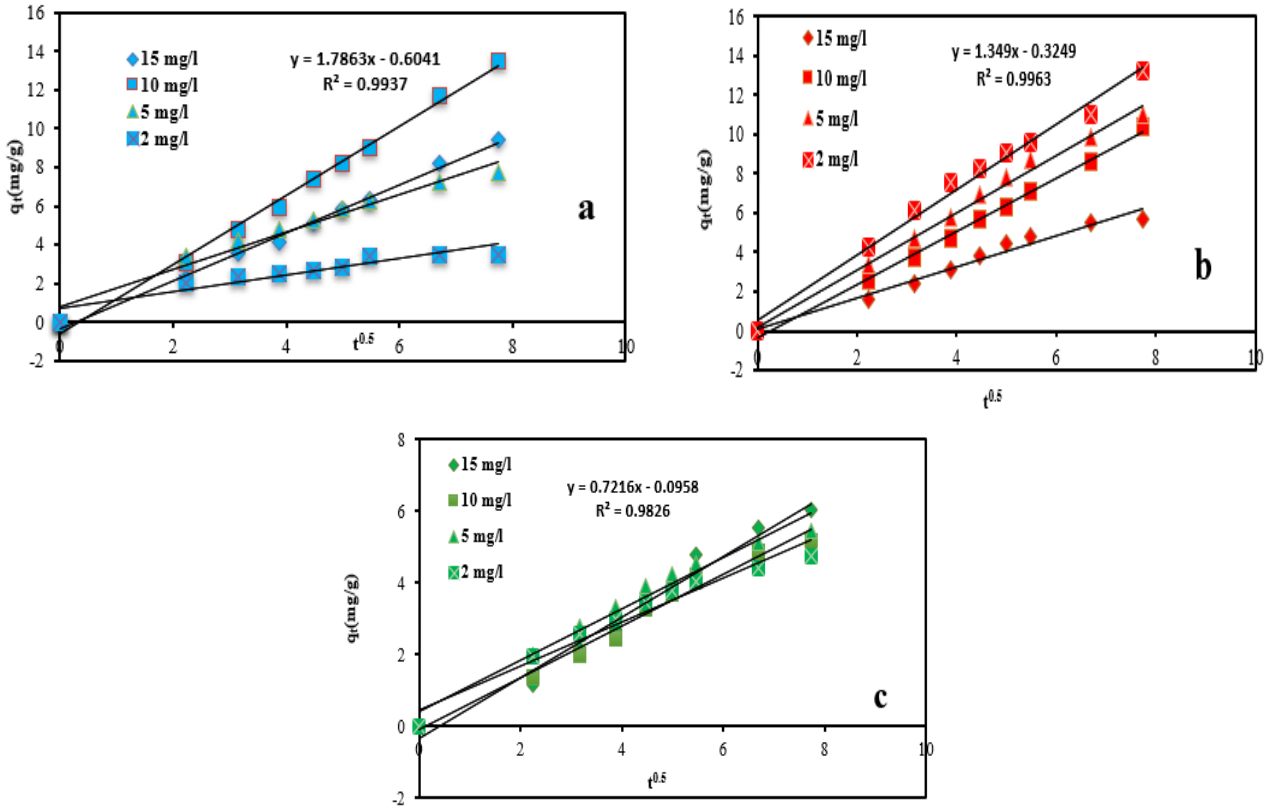

Fig. 12. The intraparticle diffusion at a different initial concentration of CIP adsorption (Temp 40C, 300 rpm, and 60 min) onto (a) Fe.NPs adsorbent dose of 0.5 g, pH10.(b) Cu.NPs sorbent dose of 0.75 g, pH4, and (c)Ag.NPs sorbent dose of 1 g, pH4.

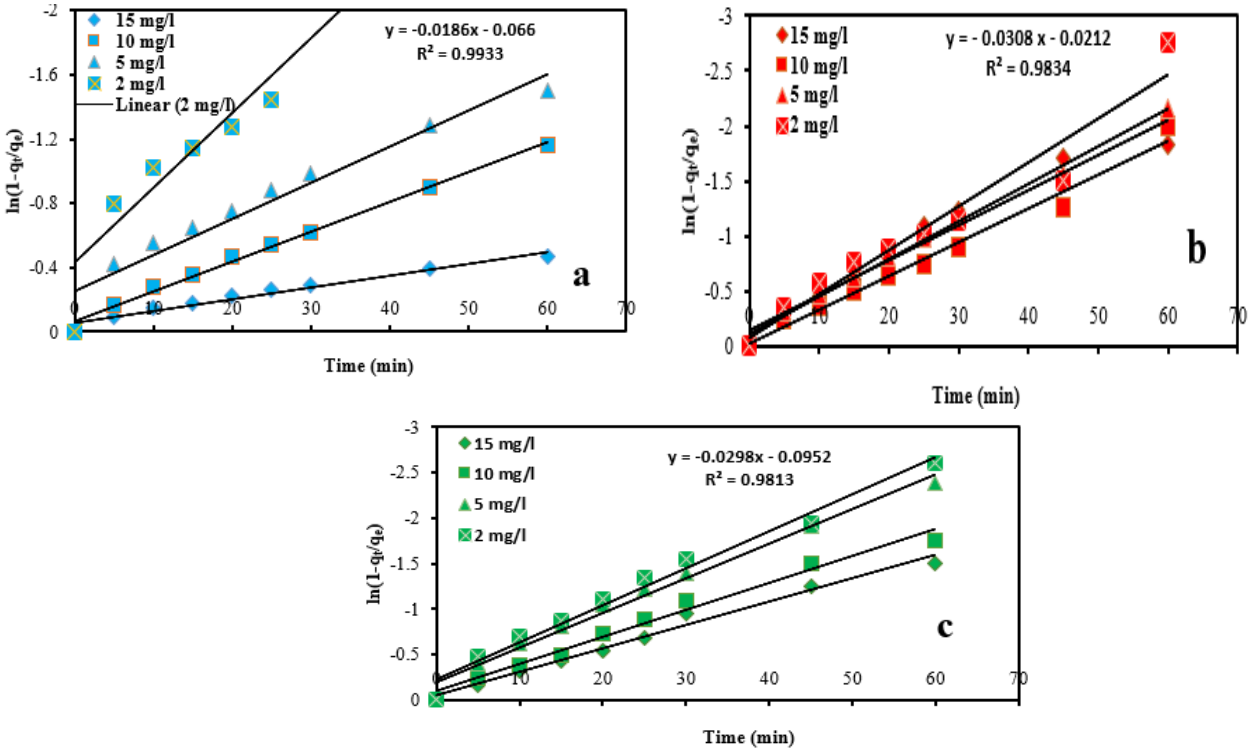

Fig. 13. The liquid diffusion at a various concentration of CIP adsorption (Temp 40C, 300 rpm, and 60 min) onto (a) Fe.NPs adsorbent dose of 0.5 g, pH10.(b) Cu.NPs adsorbent dose of 0.75 g, pH4, and (c)Ag.NPs adsorbent dose of 1 g, pH4.

5. Adsorption Isotherm

Langmuir, Freundlich, Temkin, [52][47] and Dubinin Isotherm [53] [22], have all modeled ciprofloxacin; the equations for these models are listed below.

Langmuir:

$$\frac{1}{q_e} = \frac{1}{q_{max}} K_L \left(\frac{1}{C_e}\right) + \frac{1}{q_{max}} \quad \dots (5)$$

Separation factor or dimensionless constant (RL)

$$R_L = \frac{1}{1 + bC_o} \quad \dots (6)$$

Freundlich:

$$Log\ q_e = \frac{1}{n} \log C_e + \log K_F \quad \dots (7)$$

Temkin:

$$q_e = \frac{R_T}{B_T} ln\ C_e + \frac{R_T}{B_T} \ln K_F \quad \dots (8)$$

Dubinin:

$$\ln q_e = \ln q_m - \beta \varepsilon^2 \quad \dots (9)$$

$$\varepsilon = \ln RT\ (1+\frac{1}{C_e}\ ) \quad \dots (10)$$

$$E + \frac{1}{\sqrt{-2\beta}} \quad \dots (11)$$

5.1 Langmuir model

Figure (14a-c) shows the plots of various models, where qmax and kL are constants of Langmuir model. These values were calculated using the slope and intercept of the presented graph, 1/qe vs 1/Ce. As demonstrated in Tables (5), (6), and (7), Langmuir isotherms define the values where (R2) Langmuir is greater than other models and homogenous adsorbent surfaces with the very same adsorbent surface are in Langmuir (7). Tables (5), (6), and (7) illustrate the constant b of Langmuir, which was set at 25.125 for Fe.NPs, 22.0925 for Cu.NPs, and 0.3643 for Ag.NPs (7). When (RL > 1), linear (RL = 1), favorable (RL 1), or irreversible (RL = 0), RL is a dimensionless constant and is commonly used as a separating factor for the RL indicator values and unfavorable adsorption. The RL values for CIP adsorption on "Fe.NPs, Cu.NPs, and Ag.NPs were (0.02217-0.0033), (0.00452-0.00451), and (0.2504-0.1793), respectively, and while these values indicated favorable CIP adsorption on adsorbents, they also gave erroneous values between 0 and 1. The maximal absorption (qmax.) of CIP per gram of Fe.NPs, Cu.NPs, and Ag.NPs was 9.95024, 8.3822, and 8.5034mg, respectively. For all adsorbents, the data fit well with the Langmuir isotherm, indicating a homogeneous surface supply of active sites on the adsorbent. A similar observation was reported by [11] [3].

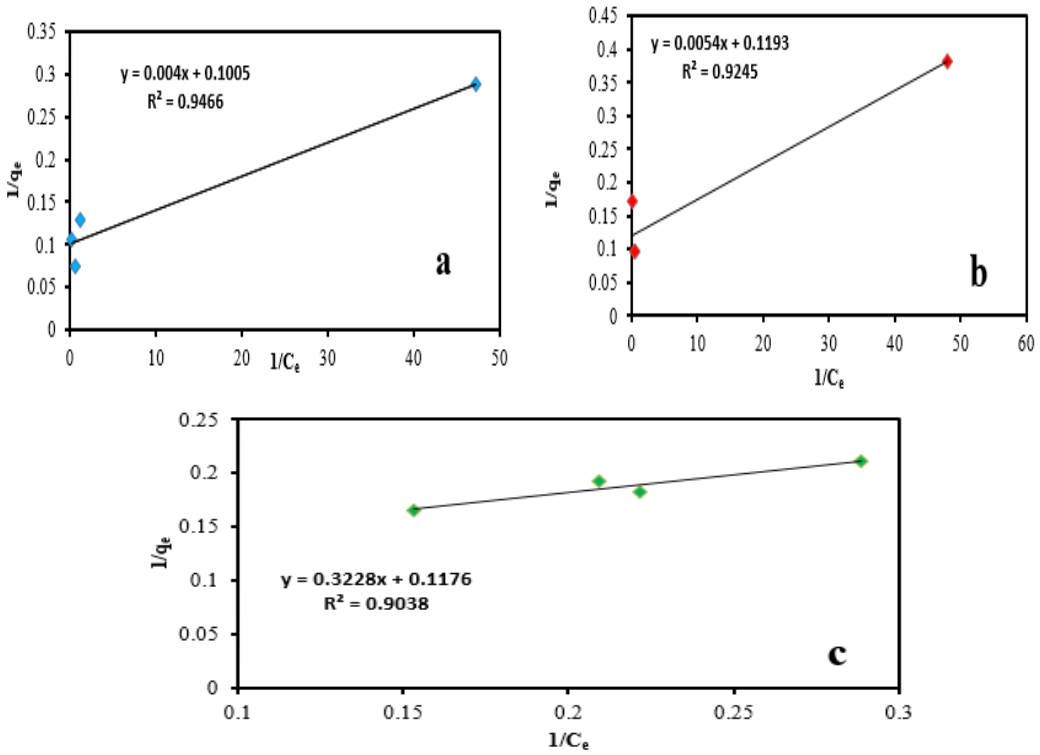

Fig. 14. The plot showing the Langmuir isotherm model at a different initial concentration of CIP adsorption (Temp 40C, 300 rpm, and 60 min) onto (a) Fe.NPs dose of 0.5 g, pH10.(b) Cu.NPs dose of 0.75 g, pH4, and (c)Ag.NPs dose of 1 g, pH4.

5.2 Freundlich isotherm model

The Freundlich isotherm is an experimental equation that considers a multi-layer sorption system on a heterogeneous surface, with the values)kF(and n confirming favorable sorption. From the plotted graph of log qe vs. log Ce, the slope and intercept were estimated as shown in Figure (15a-c). The n constants affect adsorption favorability, and " values of n between 2 and 10 are generally satisfactory, while values between 1 and 2 are difficult, and adsorption characteristics less than 1 indicate poor adsorption" (n = 4.9417, 4.7236, 2.7078) as shown in Tables (9), (10), (11) indicate acceptable adsorption [51].

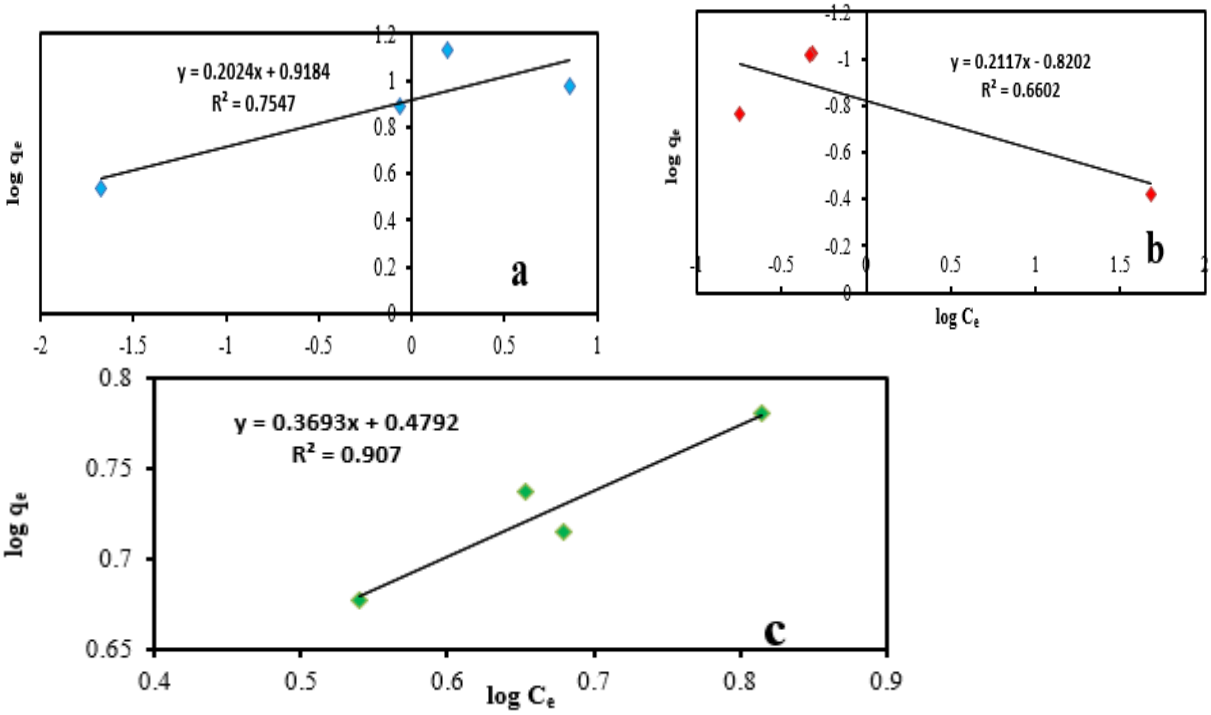

Fig. 15. The plot showing the Freundlich isotherm model at a different initial concentration of CIP adsorption (Temp 40C, 300 rpm, and 60 min) onto (a) Fe.NPs dose of 0.5 g, pH10.(b) Cu.NPs dose of 0.75 g, pH4, and (c)Ag.NPs dose of 1 g, pH4.

5.3 Temkin isotherm model

The maximum binding energy and heat of sorption coefficients are "KT (L/g) and BT (kJ/mol)". The slope and intercept of a plotted qe graph vs. ln Ce were used to get the KT and BT values (16a-c). The KT and BT values represent minute changes in sorption heat and solid interactions between adsorbent and adsorbate, as seen in Tables (8), (9), and (10).. Tables (8), (9), and (10), together with the required coefficient of correlation, and the low correlation coefficient R2 indicates that the model has no applicability.

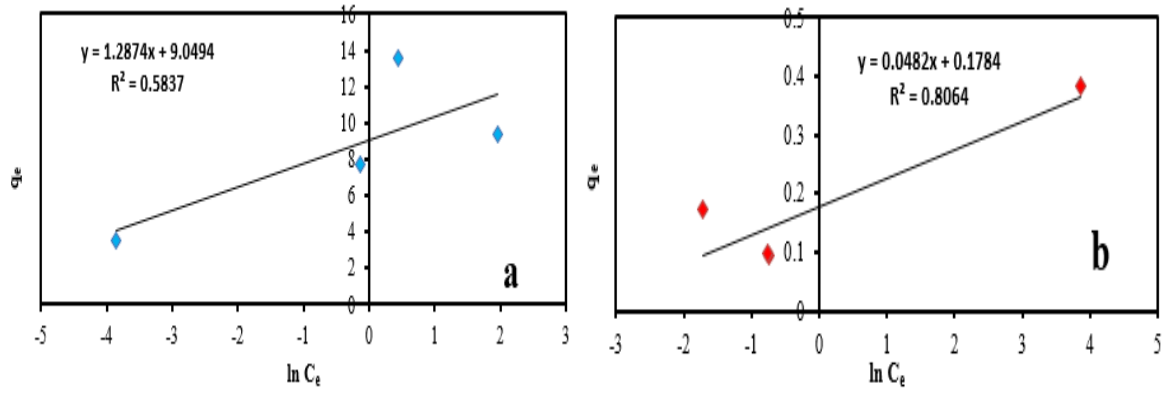

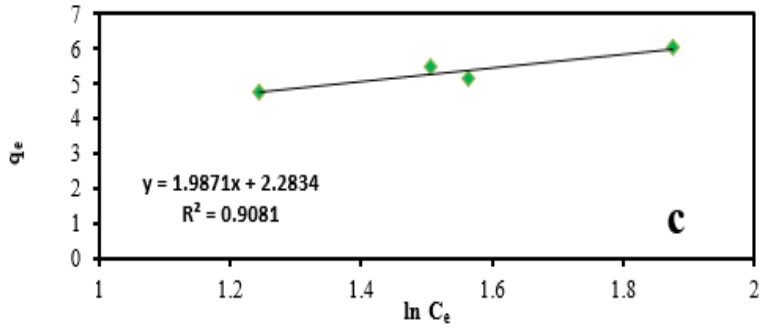

Fig. 16. The plot showing the Temkin isotherm model at a different initial concentration of CIP adsorption (Temp 40C, 300 rpm, and 60 min) onto (a) Fe.NPs sorbent dose of 0.5 g, pH10.(b) Cu.NPs sorbent dose of 0.75 g, pH4, and (c)Ag.NPs adsorbent dose of 1 g, pH4.

5.4 Dubinin isotherm model

As demonstrated in Tables (5), (6), and (7), The values qe and describe the degree and mean sorption energy per mole of adsorbate, which may be calculated from the slope and intercept of the graph plotted at ln qe versus Ɛ2 .Figure (17a-c). For "Fe.NPs, Cu.NPs, and Ag.NPs", the E values were (0.8461, 1.7205, and 3.8727 kJ/ mol, respectively, indicating physical adsorption E8 kJ/ mol, while E lies between (8-16) denotes chemical adsorption [55][56]. Because the R2 value is higher for all adsorbents, we can use this model. Figures (15a-c), (16a-c), (17a-c), and (18a-c) show the "adsorption isotherms" derived by four models, as well as "CIP experimental" data, and it is obvious that the Langmuir and Dubinin techniques were closer fits in terms of R2.

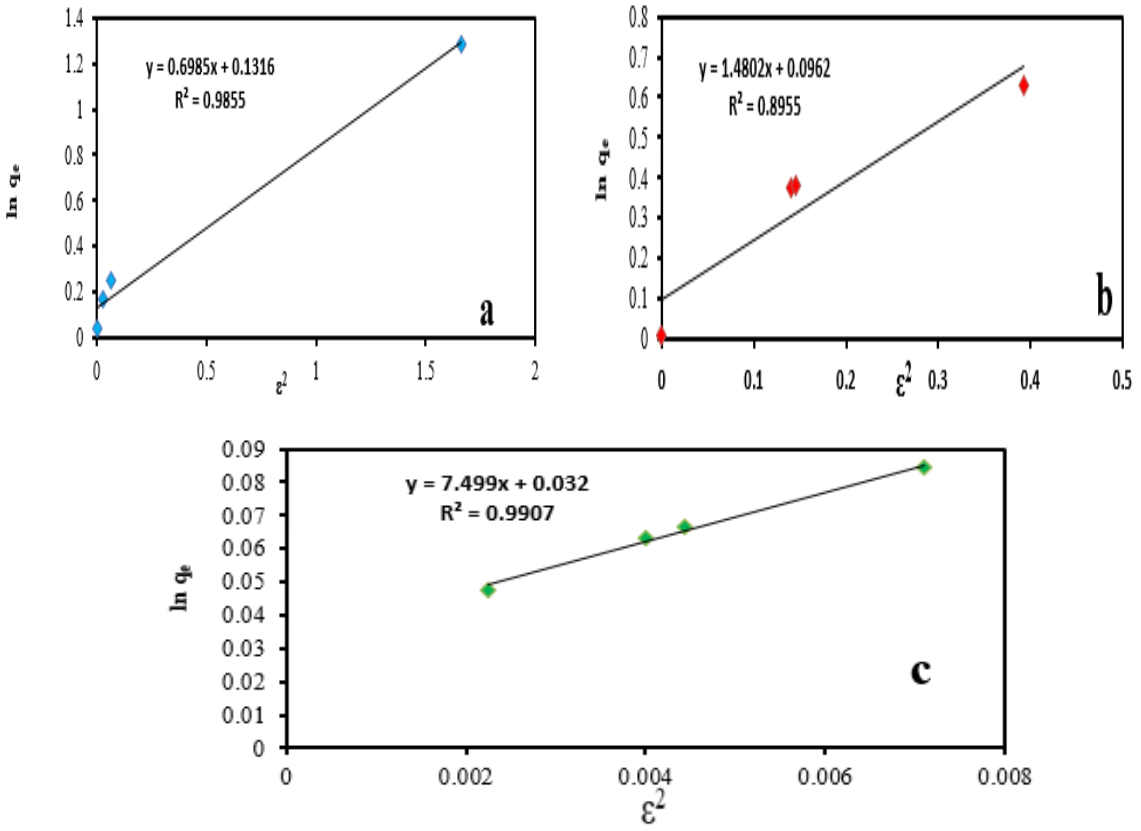

Fig. 17. The plot showing the Dubinin isotherm model at a different concentration of CIP adsorption (Temp 40C, 300 rpm, and 60 min) onto (a) Fe.NPs dose of 0.5 g, pH10.(b) Cu.NPs dose of 0.75 g, pH4, and (c)Ag.NPs dose of 1 g, pH4

Table 5,
Isotherm parameters values of Fe-NPs.

Langmuir			**Freundlich**		
q_{max} (mg g^{-1})	**B (L mg^{-1})**	**R^2**	**k_F**	**n**	**R^2**
9.95	25.13	0.947	8.287	4.941	0.755
Temkin			**Dubinin**		
K_T(L/g)	**B_T (kJ/mol)**	**R^2**	**Qm (µg/g)**	**E (kJ/mol)**	**R^2**
7.029	0.258	0.5837	1.141	0.846	0.986

Table 6,
Isotherm parameters values of Cu-NPs.

Langmuir			**Freundlich**		
q_{max} (mg g^{-1})	**B (L mg^{-1})**	**R^2**	**k_F**	**n**	**R^2**
8.3822	22.0925	0.9245	0.1512	4.7236	0.6602
Temkin			**Dubinin**		
K_T(L/g)	**B_T (kJ/mol)**	**R^2**	**Qm (µg/g)**	**E (kJ/mol)**	**R^2**
40.4976	6.8995	0.8064	1.1009	1.7205	0.8955

Table 7,
Isotherm parameters values of Ag-NPs.

Langmuir			**Freundlich**		
q_{max} (mg g^{-1})	**B (L mg^{-1})**	**R^2**	**k_F**	**n**	**R^2**
8.503	0.363	0.903	3.013	2.708	0.907
Temkin			**Dubinin**		
K_T(L/g)	**B_T (kJ/mol)**	**R^2**	**Qm (µg/g)**	**E (kJ/mol)**	**R^2**
0.167	3.155	0.908	1.033	3.873	0.991

6. Adsorption Thermodynamic

At 298, 303, 313, and 323 K, the adsorption behaviors of various concentrations of" CIP onto Fe.NPs, Cu.NPs, and Ag.NPs" were censoriously investigated, and the thermodynamic parameters of Gibbs free energy ,entropy and enthalpy were obtained using equations 12 to 16. [56], [57]:

$$\Delta G \circ = -RT \ln K_c \quad \ldots(12)$$

$$K_c = \frac{q_e}{C_e} \quad \ldots(13)$$

$$\Delta G \circ = \Delta H - T.\Delta S \circ \quad \ldots(14)$$

$$\ln \frac{C_t}{C \circ} = -k_{obs} t \quad \ldots(15)$$

$$\ln K_{obs} = \ln A - \frac{E_a}{RT} \quad \ldots(16)$$

Using ln Kc values for various temperatures, the Gibbs free energy (ΔG0) was calculated. According to Eq.19, the slope and intercept at ΔH0 and ΔS0 of the graph of ΔG0 vs T. Figure can be used to determine "enthalpy (ΔH0) and entropy (ΔS0)" (18a-c). Tables (8), (9), and (10) show the free energy, enthalpy, and entropy values for iron, copper, and silver nanoparticles. The positive enthalpy (ΔH0) value demonstrated endothermic sorption and favorable, indicating the spontaneous nature of CIP adsorption onto Fe.NPs, Cu.NPs, and Ag.NPs [58], [56]. During the adsorption process, positive entropy change determines the increase in disruption at liquid / solid interfaces [58]. Eq.16 was used to compute the activation energy, in which A represents the "Arrhenius factor, R represents the gas constant (8.314 J / mol.K)", K represents the temperature in kelvin, Ea represents the activation energy (kJ/mol), and kobs (min-1) represents the rate constant Eq.15 [59], [34]. The intercept and slope of ln (Ct/C0) and the time t (min) were used to calculate these values. For "Fe.NPs, Cu.NPs, and Ag.NPs", the straight line of ln kobs versus 1 / T Figure (19a-c) deviates by" 17.66 kJ / mol, 13.22 kJ / mol, and 14.06 kJ / mol", respectively, Diffusion-controlled processes are indicated by an activation energy (Ea) value greater than 21 kJ / mol, whereas chemically controlled processes are indicated by an Ea value less than 21 kJ / mol. [59].

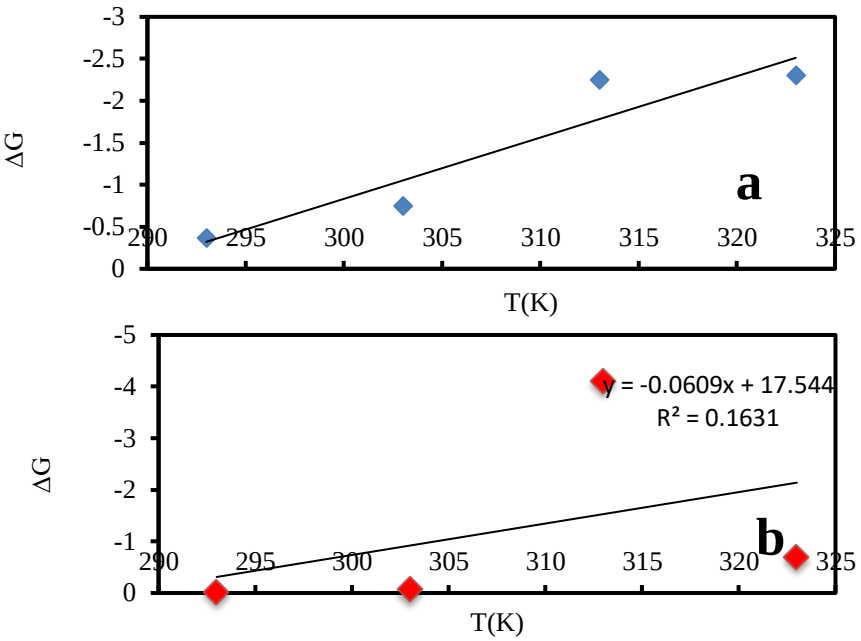

Fig.18. Relationship between ΔG^0 and T of CIP adsorption onto (a) "Fe.NPs at initial concentrations of 10 mg/L, pH=10, and 300 rpm for adsorption of CIP with a dose of 0.5 g and 60 min, (b) Cu.NPs at initial concentrations of 10 mg / L, pH=4, and 300 rpm for adsorption of CIP with a dose of 0.75 g"

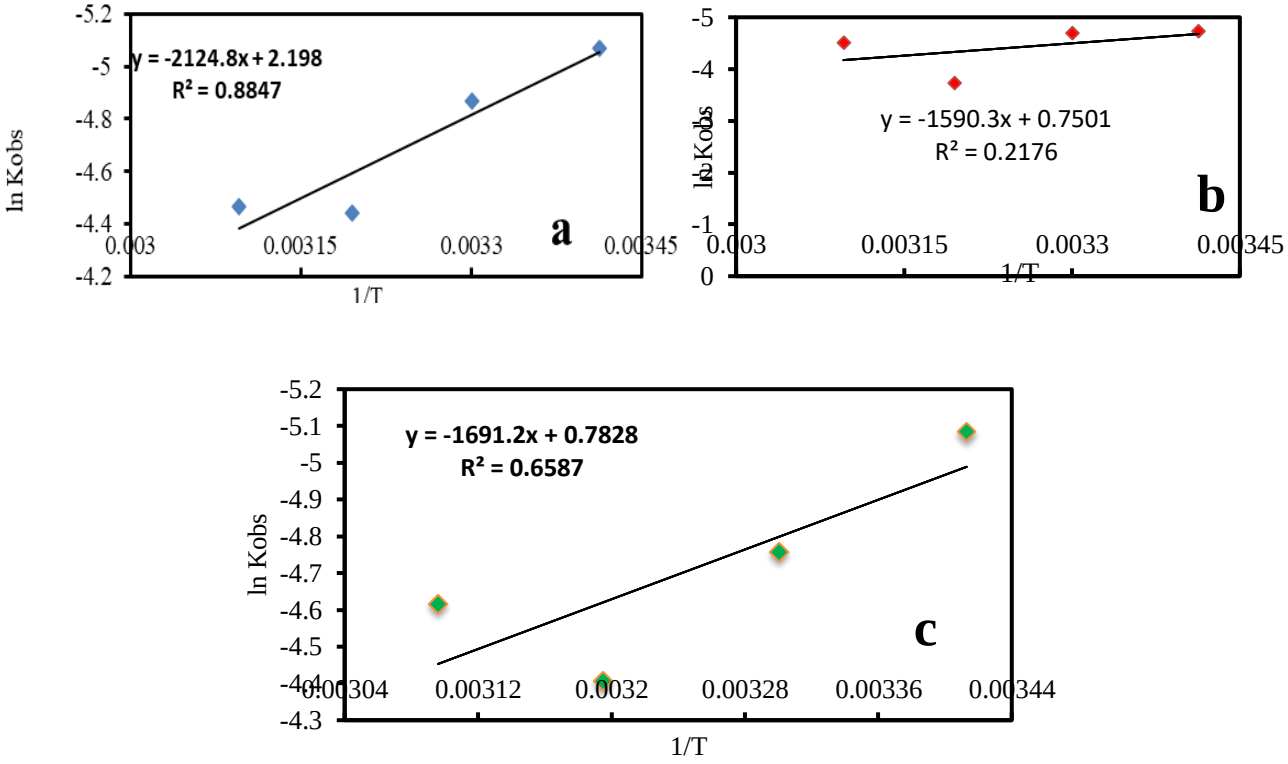

Fig. 19. "Relationship between ln kob against 1 / T to caculate Ea at concentrations of 10 mg / L, and 300 RPM , 60 min for adsorption dose of CIP on to (a) Fe.NPs with a dose of 0.5 g and pH10, (b) Cu.NPs with a dose of 0.75 g and pH4, and (c) Ag.NPs with a dose of 1 g and pH4"

Table 8,
Thermodynamic study of CIP adsorption onto Fe.NPs (CIP Conc.=10 mg/L, Fe.NPs dosage = 0.5 g, contact time= 60 min, and pH=10).

ΔG^0 (KJ/mol)				ΔH^0 (KJ/mol)	ΔS^0 (KJ/mol.K)
T=20°C	T=30°C	T=40°C	T=50°C	21.067	0.073
-0.367	-0.749	-2.249	-2.301		

Table 9,
Thermodynamic study of CIP adsorption onto Cu.NPs (CIP conc.= 10 mg/L, Cu.NPs dosage= 0.75 g, contact time= 60 min, and pH=4).

ΔG^0 (KJ/mol)				ΔH^0 (KJ/mol)	ΔS^0 (KJ/mol.K)
T=20°C	T=30°C	T=40°C	T=50°C	17.544	0.061
-0.017	-0.069	-4.108	-0.701		

Table 10,
Thermodynamic study of CIP adsorption onto Ag.NPs (CIP conc.=10 mg/L, Ag.NPs dosage= 1 g, contact time= 60 min, and pH=4).

ΔG^0 (KJ/mol)				ΔH^0 (KJ/mol)	ΔS^0 (KJ/mol.K)
T=20°C	T=30°C	T=40°C	T=50°C	12.713	0.042
0.516	-0.069	-0.959	-0.593		

5. Conclusions

Three adsorbents Fe.NPs, Cu.NPs, and Ag.NPs were characterized using advanced techniques such as SEM, AFM, BET, zeta potentials, and FT-IR, with the results indicating that nanoparticles had favorable effects in the adsorption process. Several parameters were studied to optimize the adsorption process, including, contact time, pH, temperature, and initial antibiotic concentration, and the best value of this parameter was pH10, 60 min, 10 mg/L, 40°C, and 0.5 g/L dosages for Fe.NPs, pH4, 60 min, 10 mg/L, 40°C, and 0.75 g/L for Cu.NPs, and finally pH4, 60 min, 10 mg/L, 40°C, and 0.75 g/L for Ag.NPs. The isothermal study showed the best-fitting models for the adsorbent Fe.NPs and Cu.NPs were the Langmuir and Dubinin models, respectively, whereas the best-fitting models for the adsorbent Ag.NPs were the Dubinin and Temkin models. Both the endothermal nature and the spontaneous nature of the sorption process were mentioned by the thermodynamic element. When ΔG0 is negative, the nature of adsorption was spontaneous and feasible for all nanoparticles. Finally, Fe.NPs was the most appropriate adsorbent compared with Cu.NPs and Ag.NPs in the order of "Fe.NPs > Cu.NPs > Ag.NPs".

References

[1] C. A. Igwegbe, S. N. Oba, C. O. Aniagor, A. G. Adeniyi, and J. O. Ighalo, "Adsorption of ciprofloxacin from water: A comprehensive review," *J. Ind. Eng. Chem.*, vol. 93, pp. 57–77, 2021, doi: 10.1016/j.jiec.2020.09.023.

[2] N. Genç and E. C. Dogan, "Adsorption kinetics of the antibiotic ciprofloxacin on bentonite, activated carbon, zeolite, and pumice," *Desalin. Water Treat.*, vol. 53, no. 3, pp. 785–793, 2015, doi: 10.1080/19443994.2013.842504.

[3] M. A. Asghar *et al.*, "Iron, copper and silver nanoparticles: Green synthesis using green and black tea leaves extracts and evaluation of antibacterial, antifungal and aflatoxin B1 adsorption activity," *LWT - Food Sci. Technol.*, vol. 90, no. January, pp. 98–107, 2018, doi: 10.1016/j.lwt.2017.12.009.

[4] X. Weng, L. Huang, Z. Chen, M. Megharaj, and R. Naidu, "Synthesis of iron-based nanoparticles by green tea extract and their degradation of malachite," *Ind. Crops Prod.*, vol. 51, pp. 342–347, 2013, doi: 10.1016/j.indcrop.2013.09.024.

[5] N. Sharma and N. Dhiman, "Kinetic and Thermodynamic Studies for Ciprofloxacin Hydrochloride Adsorption from Aqueous Solution on CuO Nanoparticles," vol. 10, no. 5, pp. 98–106, 2017.

[6] M. Batool, "Degradation of Malachite Green by Green Synthesized Copper Nanoparticles

by Using Aloe Barbadensis Leaf Extracts," *Arch. Nanomedicine Open Access J.*, vol. 1, no. 2, pp. 29–34, 2018, doi: 10.32474/anoaj.2018.01.000108.

[7] C. Raju, S. Nooruddin, and K. S. Babu, "Studies on leaf extract mediated synthesis of copper nanoparticles for the removal of bromo cresol green dye from synthetic waste waters," *Ijsetr*, vol. 6, no. 10, pp. 1404–1411, 2017.

[8] M. Batool, M. Z. Qureshi, F. Hashmi, N. Mehboob, and W. M. Daoush, "Adsorption of Congo red (acid red 28) azodye on biosynthesized copper oxide nanoparticles," *Asian J. Chem.*, vol. 31, no. 3, pp. 707–713, 2019, doi: 10.14233/ajchem.2019.21752.

[9] [M. Leili, M. Fazlzadeh, and A. Bhatnagar, "Green synthesis of nano-zero-valent iron from Nettle and Thyme leaf extracts and their application for the removal of cephalexin antibiotic from aqueous solutions," *Environ. Technol. (United Kingdom)*, vol. 39, no. 9, pp. 1158–1172, 2018, doi: 10.1080/09593330.2017.1323956.

[10] I. Ali, Z. A. AL-Othman, and A. Alwarthan, "Green synthesis of functionalized iron nano particles and molecular liquid phase adsorption of ametryn from water," *J. Mol. Liq.*, vol. 221, pp. 1168–1174, 2016, doi: 10.1016/j.molliq.2016.06.089.

[11] H. R. Pouretedal and N. Sadegh, "Effective removal of Amoxicillin, Cephalexin, Tetracycline and Penicillin G from aqueous solutions using activated carbon nanoparticles prepared from vine wood," *J. Water Process Eng.*, vol. 1, pp. 64–73, 2014, doi: 10.1016/j.jwpe.2014.03.006.

[12] Shi, Z.-Q.; Liu, Y.-S.; Xiong, Q.; Cai, W.-W.; and Ying, G.-G. (2019). Occurrence, toxicity and transformation of six typical benzotriazoles in the environment: A review. *Science of the Total Environment*, 661, 407-421.

[13] Pouretedal. H.R.; and Sadegh, N. (2014). Effective removal of Amoxicillin, Cephalexin, Tetracycline and Penicillin G from aqueous solutions using activated carbon nanoparticles prepared from vine wood. *Journal of Water Process Engineering*, 1, 64-73.

[14] Balcioglu. I.A.; and Otker, M. (2004). Pre-treatment of antibiotic formulation wastewater by O3, O3/H2O2, and O3/UV processes. *Turkish Journal of Engineering and Environmental Sciences*, 28(5), 325-32.

[15] Davis, T.A.; Volesky, B.; and Mucci, A. (2003). A review of the biochemistry of heavy metal biosorption by brown algae. *Water Research*, 37(18), 4311-4330.

[16] Xian, Q.; Hu, L.; Chen, H.; Chang, Z.; and Zou, H. (2010). Removal of nutrients and veterinary antibiotics from swine wastewater by a constructed macrophyte floating bed system. *Journal of Environmental Management*, 91(12), 2657-2661.

[17] Ahalya, N.; Ramachandra, T.V.; and Kanamadi, R.D. (2003). Biosorption of heavy metals. *Research Journal of Chemistry and Environment*, 7(4), 71-78.

[18] Zou, C.; Jiang, W.; Liang, J.; Sun, X.; and Guan, Y. (2019). Removal of Pb(II) from aqueous solutions by adsorption on magnetic bentonite. *Environmental Science and Pollution Research*, 26(2), 1315-1322.

[19] Ghorai. S.; Sarkar. A.; and Pal. S. (2014). Rapid adsorptive removal of toxic Pb2+ ion from aqueous solution using recyclable, biodegradable nanocomposite derived from templated partially hydrolyzed xanthan gum and nanosilica. *Bioresource Technology*, 170, 578-582.

[20] De Gisi, S.; Lofrano, G.; Grassi, M.; M, Notarnicola. (2016) Characteristics and adsorption capacities of low-cost sorbents for wastewater treatment: A review. *Sustainable Materials and Technologies*, 9, 10-40.

[21] Wang, J.; Zhang, T.; Li. M.; Yang. Y.; Lu. P.; Ning. P.; and Wang, Q. (2018). Arsenic removal from water/wastewater using layered double hydroxide derived adsorbents, a critical review, RSC Advances. *Royal Society of Chemistry*, 8(40), 22694-22709.

[22] Cheng, M.; Zhang. X .; Shi. Y.; Shi, D.; Zhu, G.; and Fan, J. (2019). Highly efficient removal of ceftiofur sodium using a superior hydroxyl group functionalized ionic liquid-modified polymer. *Science of the Total Environment*, 662, 324-331.

[23] Loo, Y.Y.; Chieng, B.W.; Nishibuchi, M.; and Radu, S. (2012). Synthesis of silver nanoparticles by using tea leaf extract from *Camellia Sinensis*. *International Journal of Nanomedicine*, 7, 4263-4267.

[24] Kamar, F.H.; Nechifor, A.C.; Nechifor, G.; AL-Musawi, T.J.; and Mohammed. A.H. (2017). Aqueous phase biosorption of Pb(II), Cu(II), and Cd(II) onto cabbage leaves powder. *International Journal of Chemical Reactor Engineering*, 15(2), Article number: 20150178.

[25] Hossain. M.; Ngo, H.; Guo, W.S.; and Setiadi, T. (2012). Adsorption and desorption of

copper(II) ions onto garden grass, *Bioresource Technology*, 121, 386-395.

[26] Holan, Z.R.; and Volesky, B. (1995). Accumulation of cadmium, lead, and nickel by fungal and wood biosorbents, *Applied Biochemistry and Biotechnology*, 53(2), 133-146.

[27] Khodadadi,.M.; Al-Musawi, T.; Kamranifar, M.; Saghi, M.; and Panahi, A. (2019). A comparative study of using barberry stem powder and ash as adsorbents for adsorption of humic acid, Environmental Science and Pollution Research. *Environmental Science and Pollution Research*, 26(25), 26159-26169.

[28] Dhiman, N.; and Sharma, N. (2018). Batch adsorption studies on the removal of ciprofloxacin hydrochloride from aqueous solution using ZnO nanoparticles and groundnut (*Arachis hypogaea*) shell powder: a comparison*, Indian Chemical Engineer. *Taylor & Francis*, 61(1), 67-76.

[29] Mohammed A.A.; Brouers, F.; Samaka I.S.; and Al-Musawi T.J. (2018). Role of Fe3O4 magnetite nanoparticles used to coat bentonite in zinc(II) ions sequestration, *Environmental Nanotechnology, Monitoring & Management*, 10, 17-27.

[30] Saif, S.; Tahir, A.; and Chen, Y. (2016). Green synthesis of iron nanoparticles and their environmental applications and implications. *Nanomaterials*, 6(11), 1-26.

[31] Ali, I.; Al-Othman, Z.A.; and Alwarthan, A. (2016). Synthesis of composite iron nano adsorbent and removal of ibuprofen drug residue from water. *Journal of Molecular Liquids*, 219, 858-864.

[32] Hassan, A.K.; Rahman, M.M.; Chattopadhay, G.; and Naidu, R. (2019). Kinetic of the degradation of sulfanilic acid azochromotrop (SPADNS) by Fenton process coupled with ultrasonic irradiation or L-cysteine acceleration. *Environmental Technology & Innovation*, 15, 100380.

[33] Ali, I.; AL-Othman, Z. A.; and Alwarthan, A. (2016). Green synthesis of functionalized iron nano particles and molecular liquid phase adsorption of ametryn from water. *Journal of Molecular Liquids*, 221, 1168-1174.

[34] Wang. J.; Ma, H.; Yuan, W.; He, W.; Wang, S.; and You, J. (2014). Synthesis and characterization of an inorganic/organic-modified bentonite and its application in methyl orange water treatment. *Desalination and Water Treatment*, 52(40-42), 7660-7672.

[35] Qassim, A.W. (2015). Spectrophotometric determination of ciprofloxacin hydrochloride in pharmaceutical formulation ciproxin. *International Journal of Advanced Scientific and Technical Research*, 3(5), 135-146.

[36] [36] Sharma, N.; and Dhiman, N. (2017). Kinetic and thermodynamic studies for ciprofloxacin hydrochloride adsorption from Aqueous solution on CuO nanoparticles, 10(5), 98-106.

[37] [37] Demirezen, D.A.; Yıldız, Y.Ş.; and Yılmaz, D.D. (2019). Amoxicillin degradation using green synthesized iron oxide nanoparticles: Kinetics and mechanism analysis. *Environmental Nanotechnology, Monitoring & Management*, 11, 100219.

[38] Kumar, R.; Singh, N.; and Pandey, S.N. (2015). Potential of green synthesized zero-valent iron nanoparticles for remediation of lead-contaminated water. *International Journal of Environmental Science and Technology. Springer Berlin Heidelberg*, 12(12), 3943-3950.

[39] Asghar, M.A.; Zahir, E.; Shahid, S.M.; Khan, M.N.; Asghar, M.A., Iqbal, J.; and Walker, G. (2018). Iron, copper and silver nanoparticles: Green synthesis using green and black tea leaves extracts and evaluation of antibacterial, antifungal and aflatoxin B1 adsorption activity. *LWT*, 90, 98-107.

[40] Shahwan, T.; Sirriah, S.A.; Nairat, M.; Boyacı, E.; Eroğlu, A.E.; Scott, T.B.; and Hallam, K.R. (2011). Green synthesis of iron nanoparticles and their application as a Fenton-like catalyst for the degradation of aqueous cationic and anionic dyes. *Chemical Engineering Journal*, 172(1), 258-266.

[41] Khoshnamvand, N.; Ahmadi, S.; and Mostafapour, F. K. (2017). Kinetic and isotherm studies on ciprofloxacin an adsorption using magnesium oxide nanopartices. *Journal of Applied Pharmaceutical Science*, 7(11), 79-83.

[42] Wang, H.; Chen, L.; Weng, L.L.; Zhang, M.Y.; and Shen, Q. (2014). Surface properties and dissolution kinetics of tea polyphenols. *Journal of Adhesion Science and Technology*, 28(24), 2416-2423.

[43] Abdel-Aziz, H.M.; Farag, R.S.; and Abdel-Gawad, S.A. (2019). Carbamazepine removal from aqueous solution by green synthesis zero-valent iron/cu nanoparticles with ficus benjamina leaves extract. *International Journal of Environmental Research*, 13(5), 843-852.

[44] KSV, G.; Reddy, P.H.; Zamare, D. (2017). Green synthesis of iron nanoparticles using green tea leaves extract. *Journal of Nanomedicine & Biotherapeutic Discovery*, 7(1), 1-4.

[45] Elahimehr, Z.; Nemati, F.; and Elhampour, A. (2020). Synthesis of a magnetic-based yolk-shell nano-reactor: A new class of monofunctional catalyst by Cu0-nanoparticles and its application as a highly effective and green catalyst for A3 coupling reaction. *Arabian Journal of Chemistry*, 13(1), 3372-3382.

[46] Shih, Y.H.; Hsu, C.Y.; and Su, Y.F. (2011). Reduction of hexachlorobenzene by nanoscale zero-valent iron: Kinetics, pH effect, and degradation mechanism. *Separation and Purification Technology*, 76(3), 268-274.

[47] Mohammed, A.A.; Najim, A.A.; Al-Musawi, T.J.; and Alwared, A.I. (2019). Adsorptive performance of a mixture of three nonliving algae classes for nickel remediation in synthesized wastewater. *Journal of Environmental Health Science and Engineering*, 17(2), 529-538.

[48] Ye, S.; Lv, X.; and Zhou, A. (2009). In vitro evaluation of the efficacy of sodium humate as an aflatoxin b1 adsorbent. *Australian Journal of Basic and Applied Sciences*, 3(2), 1296-1300.

[49] Wu, Q.; Li, Z.; Hong, H.; Yin, K.; and Tie, L. (2010). Adsorption and intercalation of ciprofloxacin on montmorillonite. *Applied Clay Science*, 50(2), 204-211.

[50] Weng, X.; Huang, L.; Chen, Z.;Megharaj,M.; and Naidu, R. (2013). Synthesis of iron-based nanoparticles by green tea extract and their degradation of malachite. *Industrial Crops and Products*, 51, 342-347.

[51] Gai, W. Z.; Deng, Z. Y.; and Shi, Y. (2015). Fluoride removal from water using high-activity aluminum hydroxide prepared by the ultrasonic method. *RSC Advances*, 5(102), 84223-84231.

[52] Kowanga, K. D.; Gatebe, E.; Mauti, G. O.; and Mauti, E. M (2016). Kinetic , sorption isotherms , pseudo-first-order model and pseudo-second-order model studies of Cu (II) and Pb (II) using defatted Moringa oleifera seed powder. *The journal of phytopharmacology*, 5(2), 71-78.

[53] Hassan, A.K.; Al-Kindi, G.Y.; and Ghanim, D., (2020). Green synthesis of bentonite-supported iron nanoparticles as a heterogeneous Fenton-like catalyst: Kinetics of decolorization of reactive blue 238 dye. *Water Science and Engineering*, 13(4), 286-298.

[54] Leili, M.; Fazlzadeh, M.; and Bhatnagar, A. (2018). Green synthesis of nano-zero-valent iron from Nettle and Thyme leaf extracts and their application for the removal of cephalexin antibiotic from aqueous solutions. *Environmental Technology*, 39(9), 1158-1172.

[55] Raju, C.; Nooruddin, S.; and Babu, K.S. (2017). Studies on leaf extract mediated synthesis of copper nanoparticles for the removal of bromo cresol green dye from synthetic waste waters. *International Journal of Science, Engineering and Technology Research (IJSETR)*, 6(10), 1404-1411.

[56] Ghadim, E.E.;Manouchehri, F.; Soleimani, G.; Hosseini, H.; Kimiagar, S.; and Nafisi, S. (2013). Adsorption properties of tetracycline onto graphene oxide: Equilibrium, kinetic and thermodynamic studies. *PLoS ONE*, 8(11): e79254.

[57] Murcia-Salvador, A..; Pellicer, J.A.; Fortea, M.I.; Gómez-López, V.M.; Rodríguez-López, M.I.; Núñez-Delicado, E.; and Gabaldón, J.A. (2019). Adsorption of Direct Blue 78 using chitosan and cyclodextrins as adsorbents. *Polymers*, 11(6), 1003.

[58] Homem, V., Alves, A. and Santos, L. (2010). Amoxicillin removal from aqueous matrices by sorption with almond shell ashes. *International Journal of Environmental Analytical Chemistry*, 90(14-15), 1063-1084.

[59] Liu, X.; Chen, Z.; Chen, Z.; Megharaj, M.; and Naidu, R. (2013). Remediation of Direct Black G in wastewater using kaolin-supported bimetallic Fe/Ni nanoparticles. *Chemical Engineering Journal*, 223, 764-771.

إزالة المضاد الحيوي السيبروفلوكساسين من المحلول المائي باستخدام ثلاث جسيمات نانوية معدنية تم تصنيعها بالطريقة الخضراء

عبد المالك ميلاد شاكر* نجاح المحنة**

محمد عبد عطية السراج* احمد خضير حسان**** فاطمة قاسم كاظم*****

زينب عادل محمود**** عزة هاشم عباس*******

* جامعة المرقيب / ليبيا

**الجامعة الألمانية للتكنولوجيا في عمان / عمان

، **، ****** قسم الهندسة الكيميائية الاحيائية/ كلية الهندسة الخوارزمي/ جامعة بغداد/ بغداد/ العراق

**** دائرة بحوث البيئة والمياه/ وزارة العلوم والتكنولوجية/ بغداد/ العراق

*******جامعة نزاربابيف/ كازاخستان

*البريد الالكتروني: Dr_Eng.Malik@Yahoo.Co.Uk

**البريد الالكتروني:najah.almhanna@gutech.edu.com

***البريد الالكتروني: atiya@kecbu.uobaghdad.edu.iq

****البريد الالكتروني:ahmedkhh71@gmail.com

*****البريد الالكتروني:qaf2622@gmail.com

******البريد الالكتروني:Zainab.amahmoud@gmail.com

*******البريد الالكتروني:azza.hashim@nu.edu.kz

الخلاصة

تبحث هذه الدراسة إمكانية إزالة السيبروفلوكساسين (CIP) من محلول مائي باستخدام ثلاثة أنواع من الجسيمات النانوية المحضرة بالطريقة الخضراء مثل جسيمات الحديد النانوية (Fe. NPs) وجسيمات النحاس النانوية (Cu. NPS) وجسيمات الفضة النانوية (Ag. NPS). تم توصيف الجسيمات النانوية المحضرة باستخدام طرق تحليل مختلفة ووفقًا لنتائج التوصيف فأن الجسيمات النانوية التي تم تحضيرها تمتلك شكل كرة وبأحجام تتراوح من 85 و47 و 32 نانومترًا ومساحة سطحها 2.1913 و 1.6562 و 1.2387 متر مربع / غرام لكل من Fe. NPs، Cu. NPs و Ag. NPs ، على التوالي. تمت دراسة تأثيرات العوامل المختلفة على إزالة السيبروفلوكساسين مثل الأس الهيدروجيني والتركيز الأولي للسيبروفلوكساسين ودرجة الحرارة وجرعة الجسيمات النانوية والوقت. أظهرت النتائج أنه تمت إزالة 10 ملغرام / لتر من السيبروفلوكساسين بنسبة 100٪ و92٪ و79٪ خلال 180 دقيقة باستخدام Fe. NPs و Cu. NPs و Ag. NPs على التوالي. بالإضافة إلى ذلك، تمت دراسة النماذج الحركية للامتصاص وآلية إزالة السيبروفلوكساسين وأظهر الدراسات أن الية الامتزاز كانت فيزيائية بطاقة 0.846 كيلو جول / مول و1.720 كيلو جول / مول و 3.872 كيلو جول / مول بينما طاقات التنشيط 17.660 كيلو جول / مول و 13.221 كيلو جول/مول و 14.060 كيلو جول/مول لكل من Fe. NPs و Cu. NPs و Ag. NPs على التوالي. تشير دراسة حركيات العملية الى ان عملية الامتزاز تخضع لنموذجا من الدرجة الأولى. تم تحليل البيانات الخاصة بالامتزاز باستخدام نماذج Langmuir وFreundlich وTemkin وDubinin. بالإضافة إلى دراسة الديناميكية الحرارية التي اشارت إلى أن عملية الامتزاز كانت ماصه للحرارة. أظهرت جسيمات الحديد النانوية كفاءه عالية مقارنة مع جسيمات النحاس والفضة النانوية